

# Young Low-Mass Stars and Brown Dwarfs in IC 348

K. L. Luhman<sup>1</sup>

Harvard-Smithsonian Center for Astrophysics, 60 Garden St., Cambridge, MA 02138;  
 kluhman@cfa.harvard.edu

## ABSTRACT

I present new results from a continuing program to identify and characterize the low-mass stellar and substellar populations in the young cluster IC 348 (1-10 Myr). Optical spectroscopy has revealed young objects with spectral types as late as M8.25. The intrinsic  $J - H$  and  $H - K$  colors of these sources are dwarf-like, whereas the  $R - I$  and  $I - J$  colors appear intermediate between the colors of dwarfs and giants. Furthermore, the spectra from 6500 to 9500 Å are reproduced well with averages of standard dwarf and giant spectra, suggesting that such averages should be used in the classification of young late-type sources.

An H-R diagram is constructed for the low-mass population in IC 348 (K6-M8). The presumably coeval components of the young quadruple system GG Tau (White et al.) and the locus of stars in IC 348 are used as empirical isochrones to test the theoretical evolutionary models. The calculations of Burrows et al. do not appear to be consistent with the data at these earliest stages of stellar evolution. There is fair agreement between the data and the model isochrones of D'Antona & Mazzitelli, except near the hydrogen burning limit. The agreement cannot be improved by changing the conversion between spectral types and effective temperatures. On the other hand, for the models of Baraffe et al., an adjustment of the temperature scale to progressively warmer temperatures at later M types, intermediate between dwarfs and giants, brings all components of GG Tau onto the same model isochrone and gives the population of IC 348 a constant age and age spread as a function of mass. When other observational constraints are considered, such as the dynamical masses of GM Aur, DM Tau, and GG Tau A, the models of Baraffe et al. are the most consistent with observations of young systems. With compatible temperature scales, the models of both D'Antona & Mazzitelli and Baraffe et al. suggest that the hydrogen burning mass limit occurs near M6 at ages of  $\lesssim 10$  Myr. Thus, several likely brown dwarfs are discovered in this study of IC 348, with masses down to  $\sim 20$ -30  $M_J$ .

---

<sup>1</sup>Visiting Astronomer, Kitt Peak National Observatory, National Optical Astronomy Observatories, which is operated by the Association of Universities for Research in Astronomy, Inc. (AURA) under cooperative agreement with the National Science Foundation.

*Subject headings:* infrared: stars — stars: evolution — stars: formation — stars: low-mass, brown dwarfs — stars: luminosity function, mass function — stars: pre-main sequence

## 1. Introduction

Brown dwarfs have been discovered over a wide range of ages. Examples of evolved field brown dwarfs ( $\gtrsim 1$  Gyr) include the companion GL 229B (Nakajima et al. 1995; Oppenheimer et al. 1995) and the free floating Kelu 1 (Ruiz, Leggett, & Allard 1997), in addition to substellar objects identified through the near-infrared (IR) surveys of 2MASS (Kirkpatrick et al. 1999) and DENIS (Martín et al. 1997; Tinney, Delfosse, & Forveille 1997; Delfosse et al. 1997). Warmer, more luminous brown dwarfs have been found at younger ages, such as the field companion G 196-3B ( $\sim 300$  Myr; Rebolo et al. 1998) and objects in the Pleiades (125 Myr) (Stauffer, Hamilton, & Probst 1994; Martín et al. 1998, references therein) and in the youngest clusters ( $\lesssim 10$  Myr) in Orion (Hillenbrand 1997),  $\sigma$  Orionis (Béjar, Zapatero Osorio, & Rebolo 1999), Taurus (Briceño et al. 1998),  $\rho$  Oph (Luhman, Liebert, & Rieke 1997, hereafter LLR; Wilking, Greene, & Meyer 1999), IC 348 (Luhman et al. 1998b, hereafter LRLL), Chamaeleon I (Comerón, Rieke, & Neuhäuser 1999), and TW Hydrae (Lowrance et al. 1999). In a sample of candidate low-mass members of the Hyades, Reid & Hawley (1999) have also serendipitously discovered five likely pre-main-sequence (PMS) brown dwarfs possibly behind the Hyades and associated with the Taurus-Auriga star forming region. Given the relatively small numbers of these objects, it is not clear whether they are representative of brown dwarfs at a given age, mass, and environment. Larger samples of brown dwarfs are critical for understanding the formation and evolution of substellar objects.

In this study, I provide a more complete picture of brown dwarfs and low-mass stars at their earliest stages of evolution ( $< 10$  Myr). Work along these lines began with observations of V410 X-ray 3 in the L1495E region of Taurus (Luhman et al. 1998a), which is one of the first M6 objects ( $0.06\text{--}0.1 M_{\odot}$ ) discovered in a star forming region (Strom & Strom 1994). The colors from  $V$  through  $L'$  were approximately dwarf-like with no significant near-IR excess emission. The IR and optical spectra exhibited features indicative of both dwarfs and giants, a behavior that has been seen in the other young cool objects discovered subsequently (e.g., LRLL). Given its youth (1-10 Myr), proximity (300 pc), and rich, compact nature (300 stars,  $D \sim 20'$ ), IC 348 is an excellent site for expanding this work to larger numbers and later types. Recent studies of IC 348 include IR imaging (Lada & Lada 1995), optical photometry (Trullols & Jordi 1997), H $\alpha$  measurements and optical images and spectroscopy (Herbig 1998), and deeper IR photometry and optical and IR spectroscopy concentrated towards the  $5' \times 5'$  cluster core (LRLL).

I have begun to increase both the area and depth of the photometry and spectroscopy, with the goal of systematically identifying and characterizing the stellar and substellar populations within the entire cluster of IC 348. When this survey is completed, the analysis of LRLL

concerning the initial mass function (IMF), star formation history, and disk properties will be updated with better number statistics and completeness to lower substellar masses. However, with data recently collected, the known low-mass population has grown enough that the typical characteristics of young low-mass stars and brown dwarfs can be investigated.

I will describe new optical imaging and spectroscopy of low-mass candidates, discuss the optical classification of young late-type objects in comparison to field dwarfs and giants, and present spectral types for the coolest sources (M4-M8.25). I will then examine the behavior of the  $JHK$  colors relative to dwarfs and to warmer, more massive ( $\sim M0$ ,  $0.5\text{-}1 M_{\odot}$ ) classical T Tauri stars (CTTS). After estimating reddening, effective temperatures, and bolometric luminosities and constructing a Hertzsprung-Russell (H-R) diagram, the locus of objects in IC 348 and the presumably coeval components of the multiple system GG Tau (White et al. 1999, hereafter W99) will be used as empirical isochrones to test the theoretical evolutionary models and temperature scales. With these results, I discuss the likely masses and ages of the objects observed in IC 348 and suggest that the hydrogen burning limit at young ages occurs near M6.

## 2. Observations

Optical images of IC 348 were obtained with the four shooter camera at the Fred Lawrence Whipple Observatory 1.2 m telescope on 1998 September 23 under photometric conditions. The instrument contained four  $2048 \times 2048$  CCDs at a plate scale of  $0''.33 \text{ pixel}^{-1}$ , with the detectors separated by  $\sim 1'$  and arranged in a  $2 \times 2$  grid. Four positions were observed towards the center of IC 348 in dithers of a few arcminutes, covering a total area of  $25' \times 25'$ . At each position, images were obtained at  $R$  and  $I$  with exposure times of 20 min. The images were bias subtracted, divided by dome flats, registered, and combined into one image at each band. Image coordinates and photometry were extracted with DAOFIND and PHOT under the IRAF package APPHOT. The plate solution was derived from coordinates of all sources observed by Lada & Lada (1995) that appeared in the optical images and were not saturated. Saturation occurred near  $I = 16.5$  and the average completeness limits were  $R \sim 23$  and  $I \sim 21$ , with brighter limits towards the nebulosity in the cluster center. For instance, with the enhanced background, source 613 has a limit of  $R > 21.5$ . Measurements were also hampered near the bright B stars BD+31°643 and  $\alpha$  Per. A few sources detected in the IR such as 611 fell within diffraction spikes of brighter stars and could not be measured.

The  $R$ -band filter in the four shooter camera has the same shape as Cousins  $R$  but with a full width at half maximum that is 150 Å smaller. The  $I$ -band sensitivity of the four shooter is broader in wavelength than Cousins  $I$ , with a long tail to the red. Whereas Cousins  $I$  falls from 90 to 5% of the peak sensitivity from 8500 to 9000 Å, the four shooter maintains 80 and 60% at these wavelengths, with 35 and 15% at 9500 Å and 1  $\mu\text{m}$ . Standard stars calibrated in Cousins  $R$  and  $I$  by Landolt (1992) were observed at colors of  $R - I < 1.2$  and  $R - I = 2.7$ . Alternately, the transformation from the instrumental system to Cousins was modeled by convolving spectra

of M dwarfs at various types with the instrument sensitivities – detector quantum efficiencies and filter transmissions – for the four shooter and the Cousins system (Landolt 1992). The color transformation derived in this modeling agreed with the one measured from the photometry of the standards. I then modeled the effect of reddening on the uniqueness of the color correction, i.e. do a reddened M4 star and an unreddened M7 star of the same instrumental  $R - I$  have the same color in the Cousins system? The results of the modeling indicate that the reddened mid-M star can have a Cousins color that is redder than the late-type star by  $\sim 0.2$  mag, and thus the color transformation does depend on spectral type and reddening. Transformations were derived for  $A_V = 0$  and 3 and the average of the two was applied to the data set for IC 348. This photometry is used in Figure 1. A more precise color correction can be computed at a particular instrumental color if either the spectral type or the reddening is known. For the spectroscopic sample discussed in this work, the spectral types were incorporated into the modeling to produce a second set of color corrections. The resulting photometry is provided in Table 1. The measurements of  $R - I$  of Herbig (1998) agree with the data presented here for  $R - I < 1.6$ , but the colors of Herbig (1998) become systematically redder by 0.3-0.5 mag at  $R - I > 1.6$ . On the other hand, as discussed by LRLL, at  $R - I > 1.6$  the colors reported by Trullols & Jordi (1997) become progressively bluer than those of Herbig (1998) by 0.3-1.5 mag, and hence bluer than the colors presented here by up to a magnitude. The colors implied by the spectra of the reddest sources (e.g., object 405) are more consistent with the photometry reported in this work.

Photometry and coordinates for cluster members with spectral types of M4 or later are listed in Table 1. Optical and IR measurements of Herbig (1998), Lada & Lada (1995), and LRLL are included as well. The IR photometry of LRLL for sources not found in Table 1 can be obtained by contacting the author. Although the IR colors agree for sources in common between the latter studies, there is an unexplained offset of 0.2 mag in all three bands, where the photometry of LRLL is fainter than that of Lada & Lada (1995). For purposes of this work, agreement is obtained by arbitrarily subtracting 0.2 mag from the measurements of LRLL. Because the completeness limit in the Lada & Lada (1995) survey is near  $K = 14$ , the uncertainties are large ( $\pm 0.2$  mag) for the faintest sources in Table 1. The photometry of LRLL is deeper ( $K \sim 16.5$ ) and should be fairly accurate ( $\pm 0.05$  mag).

Spectra were obtained for low-mass candidates in IC 348 during a few hours of service observations with the Keck II low-resolution imaging spectrometer (LRIS; Oke et al. 1995) on 1998 August 7. The multi-slit mode of LRIS was used with the  $150 \text{ l mm}^{-1}$  grating ( $\lambda_{\text{blaze}} = 7500 \text{ \AA}$ ) and GG495 order-blocking filter. The maximum wavelength coverage of LRIS, 3800 to  $11000 \text{ \AA}$ , was provided in one grating setting centered near  $7500 \text{ \AA}$ . One slit mask covered a field of view of  $5' \times 7'$  and used slitlets  $8''$  in length and  $1''.2$  in width. This configuration produced a spectral resolution of  $20 \text{ \AA}$ . Two exposures of 25 min were obtained with a single slit mask. The spectrophotometric standard star was Feige 11, observed through a  $1''.0$  slit. After subtracting the bias from the frames and flat-fielding with internal continuum lamps, the spectra were extracted and calibrated in wavelength with the Ne and Ar lamp spectra. The data were then corrected

for the sensitivity function measured from Feige 11. These observations provided spectra for the low-mass cluster members 405, 611, and 613, in addition to several background stars.

The remainder of the data were collected at the Kitt Peak Mayall 4 meter telescope. Object 407 was observed with the 4 meter Cryogenic Camera (CryoCam) on 1998 December 22, while another  $\sim 70$  sources were observed with the 4 meter RC Spectrograph (RCSP) on 1998 December 23 and 26. Under good weather conditions, I obtained a spectrum of 407 ( $I = 19.5$ ) with the  $300 \text{ 1 mm}^{-1}$  grism ( $\lambda_{\text{blaze}} = 8010 \text{ \AA}$ ), OG550 order-blocking filter, and  $1''.7$  slit. The spectral resolution was  $12 \text{ \AA}$  and the exposure time was 40 min. Additional measurements were made for the spectrophotometric standard Hiltner 102 and the spectral type standards LHS 2065 (M9V) and LHS 2243 (M8V). During the observations with RCSP, I used the multi-slit mode to obtain spectra of 8-10 objects in each of several pointings. The slit masks projected a circular field of view that was  $5'$  in diameter. The slitlets were  $2''$  in width and the spectral resolution was  $14 \text{ \AA}$ . Spectra were obtained with the  $158 \text{ 1 mm}^{-1}$  grating ( $\lambda_{\text{blaze}} = 7000 \text{ \AA}$ ) and the OG570 order-blocking filter. The data from both RCSP and CryoCam provided wavelength coverages similar to that of the LRIS spectra. Because of moderate cirrus during most of the RCSP run, I observed with several slit masks designed for brighter stars ( $I < 16$ ), in addition to two masks that targeted faint, low-mass candidates ( $I = 17\text{-}19.5$ ). Exposures times ranged between 30 and 45 min. Hiltner 102 and two young late-type sources in Taurus, V410 X-ray 5a and V410 X-ray 6, were observed through a long slit. For each mask and long slit, exposures were taken with quartz continuum and He-Ar-Ne lamps. The data reduction procedures were the same as for the LRIS data.

### 3. Discussion

#### 3.1. Identification of Low-Mass Candidates and Determination of Cluster Membership

A color-magnitude diagram with the new  $RI$  photometry for all of IC 348 ( $25' \times 25'$ ) is shown in Figure 1. Saturation occurred at  $I \sim 16.5$  and data of Herbig (1998) were used for brighter stars within his  $7' \times 14'$  survey area. At lower masses and cooler temperatures, cluster members should become redder and fainter. The colors of M dwarfs eventually saturate near  $R - I = 2.4$  for the latest types. In selecting low-mass candidates to observe through spectroscopy, the highest priority was given to targets near the cluster core to reduce field star contamination and extend the depth of the previous study of LRLL. The sources observed spectroscopically by LRLL outlined a locus of likely cluster members clearly separated from most of the background stars. In addition, IR photometry from LRLL and Lada & Lada (1995) was combined with the optical data to help identify low-mass cluster members. Since most stars have similar near-IR colors,  $J - H$  and  $H - K$  provide rough estimates of extinction, thus distinguishing cool, low-luminosity brown dwarfs from reddened, luminous early-type stars (either cluster members or background)

that appear in the optical color-magnitude diagram. Unfortunately, at the faintest limits ( $I > 19$ ) where the most background contamination occurs, the available  $JHK$  data is sufficiently deep only in the cluster core. Actively accreting stars often have strong ultra-violet and optical excess emission that reduce the apparent  $R - I$  color while leaving  $I$  relatively unchanged. Such a star could therefore be mistakenly rejected as a background object in the selection of candidates.

Field stars are easily distinguished from low-mass cluster members with the spectroscopic data. Unlike young cool stars, foreground M dwarfs have strong absorption in Na and K (see Figs. 2-5), no signs of reddening in the spectra or colors, no IR excess emission, and little  $H\alpha$  emission ( $< 15$  Å). Only a few foreground M stars are expected towards the relatively small area covered by IC 348 (see Herbig 1998). Most background stars are rejected by their positions in the optical color-magnitude diagram. Ones that fall within the locus of cluster members are background giants, which exhibit spectra that differ greatly from late M cluster members.

The combined new and published spectroscopic samples are shown in the top panel of Figure 1. Reddened low-mass stars belonging to the cluster are scattered among the likely brown dwarfs ( $\geq M6$ ). Because of the compact nature of the cluster, there is very little contamination from foreground or background stars within the locus of cluster members. As demonstrated in the lower panel of Figure 1, there are many likely low-mass cluster members that remain to be observed spectroscopically.

### 3.2. Spectral Types

#### 3.2.1. Method of Classification

For the classification of sources in the new spectroscopic sample, spectra of standard dwarfs and giants are taken from Kirkpatrick, Henry, & McCarthy (1991), Henry, Kirkpatrick, & Simons (1994), and Kirkpatrick, Henry, & Irwin (1997). The spectral types are represented by averages of one or more stars. For M4V-M6V, they consist of: M4V=GL 213, GL 275.2A, and GL 402; M4.5V=GL 234AB and GL 268; M5V=GL 51 and GL 866AB; M5.5V=GL 65A and G 208-44AB; M6V=GL 406. The stars that are used for M7V-M9V and M5III-M9III are listed in Luhman et al. (1998a) and LLR. There are some differences in the band strengths among the standards of a given spectral type, particularly at M8 and M9 where the VO changes very rapidly. These fluctuations correspond to  $\sim 0.25$  subclass. Hence, the exact spectral type depends slightly on the choice of standards.

As illustrated in Figs. 2-5, TiO and VO give rise to several distinctive absorption features that are the primary indicators of spectral type. The spectrum of each young object was compared to the dwarfs, giants, and averages of the two (each normalized at 7500 Å) at various spectral types and reddenings until a best match was achieved. After this initial classification of the sample, all spectra at the same spectral type were dereddened to match the least reddened spectrum.

These data were compared closely and minor adjustments ( $\sim 0.25$  subclass) were made in the classifications, until a point was reached where objects of a given spectral type were identical within the noise. Because of the rapid change in optical features with lower temperatures, the relative classifications are quite precise. Typical uncertainties are  $\pm 0.25$  subclass for objects with one spectral type listed in Table 1. A larger range of possible spectral types is given for some sources. Even for data of very low signal-to-noise, the uncertainties in spectral types were no more than  $\pm 1$  subclass. Spectra previously classified in LRLL have been included with the new sample when deriving spectral types, some of which have been revised slightly from those reported by LRLL. Table 1 lists all known objects in IC 348 with classifications of M4 or later. New spectral types for earlier sources will be presented in a future study. The IR types from LRLL are given in Table 1 as well, in addition to optical types of Herbig (1998) for the two sources that were not in my optical sample. A spectral type of M5.5 was measured for the two sources in Taurus, V410 X-ray 5a and V410 X-ray 6, compared to previous optical classifications of M5 for both objects (Strom & Strom 1994) and M5.5 for 5a (Briceño et al. 1998).

### 3.2.2. Comparison to Dwarfs and Giants

While the relative spectral types of the sample in IC 348 are precise, the absolute classifications require further attention. The late-M spectroscopic standards defined to date consist of field dwarfs and giants. The optical spectra of these standards differ between luminosity classes for a given spectral type. Hence, classifications of young M objects can depend on the choice of dwarfs or giants as the standards and on the wavelength range considered. In previous studies, I have used spectra of field dwarfs and giants and averages of the two in the classification of a small number of young late-type objects, finding that the averages produce the best match. The new observations in IC 348 combined with the studies of LRLL and LLR provide spectra for a large population of young cool sources, including six objects at M8-M8.5. Because the young cool sources in this study form well-defined spectral classes, I can select objects with low reddening that are representative of each spectral class. After estimating the extinctions for these objects, the spectra are then dereddened to their intrinsic form. These data will be compared to the spectra of standard dwarfs and giants and their averages at spectral types of M5 through M8.5, thus revealing the spectral behavior of cool PMS objects and indicating the most suitable choice of standards for their classification. Similar discussions pertaining to  $K$ -band spectral features are found in LR98, LRLL, and Luhman & Rieke (1999).

The spectrum of source 277 exhibits the least extinction of the M5 objects and thus will be used to represent this spectral type upon dereddening. The two bluest spectra among slightly earlier and later spectral types are those of 266 and 163, respectively, which have similar slopes and are bluer than 277 by  $A_V \sim 1$ . It is likely that 266 and 163 have little extinction since they show the least reddened spectra out of 26 objects from M4.75-M5.25. An extinction of  $A_V > 1$  would imply that their spectra are intrinsically bluer than those of both dwarfs and giants and

the reddenings derived from  $J - H$  for 163, 266, and 277 in § 3.3 are low ( $A_V \sim 0.5 \pm 1$ ). An extinction of  $A_V = 1$  is therefore adopted for 277 and used in estimating the intrinsic spectrum. In Figure 2, the dereddened spectrum of 277 is shown with the M5 standards. To facilitate the comparison of individual features between the young star and the standards, the reddenings of the standards have been adjusted to match their 7000-8500 Å slopes to the spectrum of 277. The slope of 277 agrees well with an average of M5 dwarf and giant spectra without any such adjustment. Thus, young M5 objects appear to be redder than giants and bluer than dwarfs. The TiO strength from 7100 to 7300 Å in 277 is the same as in M5V, while weaker than in M5III, so that the average of the two luminosity classes has TiO that is slightly stronger than in 277. This young object shows very weak absorption in K and Na, similar to the giant. Although K and Na are not useful in measuring spectral types, they do clearly indicate PMS nature and cluster membership. Absorption in VO at 7900 and 8500 Å is not sensitive to gravity and is unchanged among the dwarf, giant, and young star.

In a study of the relatively unreddened V410 X-ray 3 ( $A_V \sim 0.6$ ), Luhman et al. (1998a) found that the spectral slope from 6500 to 9000 Å of this young M6 object was reproduced well by M6III, while bluer than M6V. In a different comparison in Figure 3, the spectral slopes of the standard stars and V410 X-ray 3 have been aligned through dereddening, as with source 277. The TiO absorption at 7100 to 7300 Å in the giant is slightly stronger than in the young object. The average of the dwarf and giant matches the CaH, TiO, and VO between 6900 and 7500 Å quite well, much better than either a dwarf or giant alone. The K and Na absorption and overall slope resemble a giant more than a dwarf. The VO at 7900 and 8500 Å in V410 X-ray 3 is matched by both luminosity classes.

In the sample for IC 348, there are no spectra showing low reddening and high signal-to-noise near a spectral type of M7. W99 have recently obtained high-quality data for the relatively unreddened binary components GG Tau Ba and Bb. They reported spectral types of  $M5 \pm 0.5$  and  $M7 \pm 0.5$ , respectively, where VY Peg (M7III) was used as the standard in the classifying Bb. From the optical spectra of GG Tau Ba and Bb kindly provided by R. White, I have measured spectral types that fall within the uncertainties quoted by W99. However, I find that more accurate and precise spectral types of  $M5.5 \pm 0.25$  and  $M7.5 \pm 0.25$  can be achieved from the data. As seen in Figure 3 in W99, the VO absorption at 7900 and 8500 Å is stronger in Bb than in either M7V or M7III. A better match to these features and the remainder of the spectrum is provided by an average of M7 and M8 dwarfs and giants.

The spectrum of source 405 is shown in Figure 4 with the M8 dwarf and giant standards. By applying a very small amount of reddening ( $A_V = 0.25$ ) to the standard spectra, an optimum match is obtained to the slope of 405 shortward of 8500 Å. Late M giants become progressively redder than dwarfs beyond 8500 Å and 405 is intermediate between the two. As demonstrated in Figure 4, the average of M8V and M8III clearly produces the best agreement with the spectrum of 405, particularly across the structure between 7900 and 8500 Å.

In a comparison of the spectrum of a young brown dwarf in  $\rho$  Oph (162349.8-242601, GY141) to averages of dwarf and giant spectra at M7, M8, and M9, LLR found that this object was intermediate between M8 and M9 and assigned a spectral type of M8.5. For a fixed M8.5 spectral class, the spectrum of this object is now compared to data representing a dwarf, a giant, and an average of the two in Figure 5. GY141 has strong VO at 8500 Å and a red spectral slope that resembles a giant, while the CaH, TiO, and VO short-ward of 8500 Å are reproduced well by the dwarf/giant average. The spectrum of a young M8.5 object in  $\sigma$  Ori is very similar to that of GY141 (Béjar et al. 1999), suggesting that GY141 may be representative of this PMS spectral type.

Absorption in VO at 7900 and 8500 Å is a very good indicator of spectral type in young late-type objects since it is strong, easy to detect in faint sources, and does not depend on surface gravity. Most of the other spectral features have strengths intermediate between dwarf and giant values. Indeed, straight averages of field dwarf and giant spectra reproduce the data for cool PMS sources remarkably well. Except for differences in reddening, the examples described here are generally representative of young ( $\lesssim 10$  Myr) cool objects in IC 348 and in other regions. Thus, I advocate the use of averages of dwarf and giant standards for classification of young objects at M5 and later, with the caveats for individual features discussed in this section. This choice of standards is also practical since the majority of young late-type objects discovered to date have been classified in this manner (this work, LRLL, LLR). Young sources with little reddening ( $A_V < 1$ ) and precise classifications should be used as supplemental standards.

### 3.3. Colors and Extinctions

The typical behavior of the optical and IR colors of young late-type sources is investigated in the data for IC 348, followed by a determination of the best method of deriving extinctions for such a population. Standard dwarf colors are taken from the compilation of Kenyon & Hartmann (1995) for types earlier than M0 and from the young disk populations described by Leggett (1992) for types of M0 and later. The IR colors are placed on the CIT system with relations between the Johnson-Glass and CIT systems found in Bessell & Brett (1988). Reddenings are calculated with the extinction law of Rieke & Lebofsky (1985).

The low-mass sources in IC 348 and standard dwarfs and giants are shown in a diagram of  $H - K$  versus  $J - H$  in Figure 6. With later M types,  $J - H$  colors for dwarfs remain near 0.6-0.7 while  $H - K$  colors increase from 0.15 to 0.5. Giants depart from dwarf colors near  $J - H = 0.6$  and  $H - K = 0.1$  and approach colors of 1 and 0.3 at the latest types (Bessell & Brett 1988). For each of the three ranges of spectral types in Figure 6, a reddening vector originates at the corresponding dwarf colors. The young systems in IC 348 move progressively to redder  $H - K$  with later types, closely following the dwarf behavior. The  $J - H$  colors in the least reddened objects are similar to dwarfs and bluer than giants, indicating that both IR colors of the central stars are dwarf-like.

As with higher mass CTTS, some of the low-mass objects in IC 348 show emission in excess of reddened dwarf colors. Meyer, Calvet, & Hillenbrand (1997) measured a locus of dereddened IR colors for classical T Tauri stars near M0 and modeled it in terms of star-disk systems, where the origin of this locus coincides with the unreddened colors of an M0 dwarf. At later M types, they predict that the origin will continue to follow the dwarf colors while maintaining a fairly constant slope. To test this suggestion, a fit to the CTTS locus of Meyer et al. (1997) is given in Figure 6 with the origin adjusted for each of the three spectral types. As discussed shortly, it may not be possible to measure accurate reddening from optical colors of these young cool objects. Hence, it is difficult to deredden the IR colors for comparison to the CTTS locus. The large photometric uncertainties and the small number of sources with significant  $H - K$  excesses provide further obstacles in determining the intrinsic colors of low-mass CTTS. However, it is apparent that at the latest types the average observed colors fall below the CTTS locus, a trend that would become more pronounced if the colors were dereddened. In other words, these systems seem to have significant color excesses at  $H - K$  but not  $J - H$ . Relative to CTTS at higher masses, this behavior would suggest cooler emitting regions with respect to the central objects, possibly due to cooler disks, larger inner holes, or contributions from material in infalling envelopes. The latter emission source is particularly likely in object 407, which has a higher  $H - K$  excess than can be easily explained by star-disk systems (Meyer, Calvet, & Hillenbrand 1997). As seen in Figure 6, the systems with higher H $\alpha$  emission tend to show larger excesses at  $H - K$ , which is expected for more actively accreting disks. It also appears that on average the latest types show the largest excesses. However, the uncertainties in the colors are largest for the faintest, coolest objects. For instance, the anomalous colors of 432 ( $J - H = 0.9$ ,  $H - K = 0.04$ ) reported by Lada & Lada (1995) are likely due to the uncertain  $K$ -band measurement ( $\pm 0.39$  mag). A more conclusive and detailed analysis of these various issues requires more accurate  $JHK$  photometry and data at longer wavelengths.

As demonstrated by the  $J - H$  color excesses in Figure 6 ( $A_J = 2.63E(J - H)$ ), the sources at M4-M5 exhibit  $A_J = 0.2$  while the later types have  $A_J \lesssim 1$ , which is a reflection of the completeness limit of the spectroscopy and selection against reddened late-type objects. The M4-M5 stars with  $A_J < 1$  are saturated in the new  $RI$  photometry. To examine  $R - I$  and  $I - J$  for the remaining sources, the colors have been dereddened with the extinctions derived from  $J - H$  assuming intrinsic colors of dwarfs. The dereddened  $R - I$  colors are bluer than dwarf values by 0.2-0.6 mag for objects at M4-M5, which is a tendency towards giant-like colors. At later types, the young sources have colors similar to dwarfs and giants, which have comparable Cousins  $R - I$  colors for M6 and later. (It is redward of Cousins  $I$  where late M giants become redder than dwarfs.) This behavior is consistent with the spectra, where the slopes across the Cousins  $R$  and  $I$  bands are bluer than in dwarfs for M4-M6 and similar to both dwarfs and giants at later types. Because the cooler objects have low extinctions and the non-saturated M4-M5 stars are reddened, the results of this comparison are susceptible to systematic effects from the color correction. However, careful modeling of the color transformation as a function of spectral type and reddening (§ 2) indicates that the optical colors are fairly accurate ( $\pm 0.1$ ) and the blue

dereddened colors at M4-M5 should be a real effect. Comparing the optical and IR data, the dereddened  $I - J$  colors are redder than dwarf values by 0, 0.3, and 0.6 mag at M4-M5, >M5-M6, and >M6. As discussed in § 2, the IR photometry of LRLL was offset by  $-0.2$  mag to agree with the data of Lada & Lada (1995). If the reverse adjustment is made, then these color differences in  $I - J$  are reduced by 0.2 mag. A noticeable departure from dwarf colors would remain at the latest types, with  $I - J$  intermediate between that of dwarfs and giants. The spectra of the latest objects rise rapidly beyond the  $I$ -band in a similar fashion as giants, confirming the behavior of  $I - J$ . Color anomalies from  $B$  through  $J$  have also been observed in earlier type (K7-M1) PMS stars by Gullbring et al. (1998). Because dwarf and giant colors are similar in this spectral type regime, they suggest that cool companions and star spots are instead the probable causes.

To derive extinctions for stars earlier than mid-M, LRLL used  $E(R - I)$  and assumed intrinsic colors of dwarfs, with the constraint that the extinction could not produce a dereddened  $J - H$  much bluer than in dwarfs. When  $R$  and  $I$  were not available, the stars were dereddened to the dwarf colors of  $J - H$ . For the three latest sources in LRLL, the extinctions were estimated from  $I - K$  by assuming dwarf colors since this was the most accurate color for these faint objects. The new results in this study indicate that the intrinsic near-IR colors of young late-type objects are probably dwarf-like while  $I$  relative to  $J$ ,  $H$ , and  $K$  appears to be redder than in dwarfs. The  $R - I$  colors of young objects also seem to deviate from those of dwarfs, making it difficult to use  $R$  or  $I$  in measuring extinctions. Possible systematic effects in the optical color transformation for reddened late-type stars is an added concern. Unlike optical data, near-IR photometry is not susceptible to significant color corrections and the colors are consistently dwarf-like, thus extinctions are derived in this work by dereddening  $J - H$  to dwarf colors. Unfortunately, much of the near-IR data for IC 348 suffers from large photometric errors at the faintest objects. The more accurate IR data from LRLL is used when possible and the resulting extinctions are given in Table 1, which are generally consistent with the reddening implied by the spectra. Since most sources exhibit  $H - K$  excesses of  $< 0.2$  mag, the contamination of the  $J - H$  color by excess emission should be negligible. Object 407 has a large  $H - K$  excess, thus an extinction cannot be confidently derived with  $J - H$ . Cousins  $R - I$  colors are similar between dwarfs and giants at the latest M types, hence this color is used in estimating a reddening of  $A_J \sim 1$ , which is consistent with the appearance of the spectrum. Since LRLL could not measure  $H$ -band data for source 413, the  $J - K$  color was used to measure the extinction.

### 3.4. Bolometric Luminosities and Effective Temperatures

To minimize contamination from UV and IR excess emission, the  $I$  and  $J$  bands are generally preferred for estimating the bolometric luminosities of young stars. Both the photometry and the spectra indicate that  $I - J$  may be redder in young cool objects than in dwarfs. Because  $J - H$  and  $J - K$  are dwarf-like,  $J$  is likely a better choice than  $I$  for measuring luminosities. The dwarf-like near-IR colors and the fact that most of the luminosity is released in  $J$  through  $K$

suggest that the bolometric corrections for dwarfs may be satisfactory approximations for these young sources. Hence, the luminosities reported in Table 1 have been calculated by applying the dwarf bolometric corrections to the dereddened  $J$ -band data and assuming a distance modulus of 7.5. Bolometric corrections are taken from Kenyon & Hartmann (1995) for  $<\text{M}6$  and compiled from Bessell (1991), Monet et al. (1992), Tinney, Mould, & Reid (1993), and Leggett et al. (1996) for  $\geq\text{M}6$ . Given the uncertainties in the photometry, reddenings, bolometric corrections, and distance, the typical errors in the bolometric luminosities are  $\pm 0.08$  to  $0.13$  in  $\log L_{\text{bol}}$  from early K to the latest M types.

Theoretical mass tracks at low masses are mostly vertical in the H-R diagram, thus the conversion of spectral types to effective temperatures directly influences the mass estimates for young late-type objects. LR98 discussed the differences between the available temperature scales for M dwarfs, finding that the comparison of synthetic spectra to observed data by Leggett et al. (1996) produced a scale in good agreement with measurements for the eclipsing spectroscopic binaries YY Gem and CM Dra. Because the latest type in the study of Leggett et al. (1996) was M6.5, LR98 extrapolated the scale to later types assuming the same offset between the M6-M9 subclasses as found in a previous generation of spectral modeling by Kirkpatrick et al. (1993). This version of the scale of Leggett et al. (1996), given in Table 2, is consistent with newer modeling of colors at the latest M types by Leggett, Allard, & Hauschildt (1998). Since PMS stars are intermediate in surface gravity between dwarfs and giants, it is useful to consider the temperature scale for giants as well. The giant temperature scale in Table 2 is from the fit provided by van Belle et al. (1999) for types earlier than M7 and from Perrin et al. (1998) and Richichi et al. (1998) for M7 to M9. The temperatures of giants are warmer than those of dwarfs by 200-400 K, as illustrated in Figure 7.

In previous studies of young populations composed primarily of objects at mid-M and earlier, LR98, LRLL, Luhman & Rieke (1999) applied the dwarf temperature scale, while Luhman et al. (1998a) and LLR explored the effect of a warmer, more giant-like scale on mass estimates for two late M objects. For the late-type sources in IC 348 in Table 1, spectral types are converted to temperatures with the dwarf scale. In § 3.5, it will be determined if this scale or one intermediate between those of dwarfs and giants can produce agreement between the available theoretical isochrones and the empirical isochrones formed by the locus of stars in IC 348 and the components of GG Tau.

### 3.5. H-R Diagram

Using the temperatures and luminosities for objects in Table 1 ( $\geq\text{M}4$ ) and in the study of LRLL ( $<\text{M}4$ ), an H-R diagram is generated for the low-mass population in IC 348 and shown with three sets of theoretical evolutionary tracks in Figs. 8 and 9. The models include those by D'Antona & Mazzitelli (1997) (hereafter DM97), Burrows et al. (1997), and Baraffe et al. (1998) (hereafter B98) with a mixing length of  $\alpha = 1.9$ . The models of Burrows et al. (1997) shown here

are not the same as the older 1997 suite of Burrows presented in LLR, LRLL, and Luhman et al. (1998a). Burrows et al. (1997) calculated their own synthetic atmospheres, whereas the NextGen atmospheres of Allard were used in the previous generation of models. With evolutionary models, the data for a young population can be interpreted in terms of masses and ages and combined into a mass function and a star formation history. However, even the most recent models imply significantly different masses and ages for the same objects. In addition, the temperature scale for young cool stars may differ from the dwarf conversion. Therefore, meaningful estimates of masses and ages require observational constraints of the models and the temperature scale.

Luhman (1998) briefly reviewed some of the observational tests of the models at ages of  $\geq 0.1$  Gyr, which included the independently measured masses, radii, and temperatures of CM Dra and YY Gem and the empirical isochrones observed in the Pleiades and in globular clusters. In a more detailed study, Stauffer, Hartmann, & Barrado (1995) compared each set of model isochrones to the Pleiades locus and determined whether the temperature scale could be adjusted to produce agreement. While the models at evolved ages are similar to each other and in reasonable agreement with observations, at ages of  $< 10$  Myr they differ greatly and lack definitive constraints (e.g., eclipsing binaries). As a crude test at young ages ( $\sim 1$  Myr), Luhman (1998) calculated the IMF of L1495E with each set of tracks to search for anomalously large deviations from the field mass function.

### 3.5.1. Coevality as a Test of the Models

Coevality can be utilized as a constraint of the models at the youngest ages in the same way that the Pleiades locus acts as a test near 100 Myr. Binary systems should be one source of coeval stars, as explored by Hartigan, Strom, & Strom (1994) and Prato (1998). More recently, W99 have measured spectral types and photometry for the members of the quadruple system GG Tau. An H-R diagram was constructed from this data, where the presumably coeval components should form an empirical isochrone extending across a large range of spectral types (K7-M7). W99 examined several sets of models and found that the calculations of B98 with a mixing length of  $\alpha = 1.9$  could be combined with a temperature scale intermediate between those of dwarfs and giants to produce coeval ages for the components of GG Tau. These models also implied masses of DM Tau and GG Tau Aa+Ab that were in rough agreement with dynamical estimates. Using revised spectral types for GG Tau Ba and Bb (§ 3.2.2) and the reddenings and *J*-band photometry measured by W99, the luminosities of GG Tau have been calculated in the same manner as for the sources in IC 348. The luminosities agree within the uncertainties with those of W99. The revised measurements for GG Tau and the new data for IC 348 are combined in the following analysis.

### 3.5.2. GG Tau and IC 348 as Empirical Isochrones

A test of the model isochrones with data for GG Tau and IC 348 is based on the assumptions that the components of GG Tau are coeval and that luminosities are precise indicators of age. Considering the stellar densities in Taurus and separations within GG Tau, the members of this multiple system have probably formed through fragmentation rather than capture or disk instabilities, thus coevality is likely (Ghez, White, & Simon 1997). When the populations of young clusters are placed on H-R diagrams, the distribution of luminosities at a given temperature is generally interpreted in terms of an age spread. However, other factors in addition to age, such as binarity and star spots, may significantly influence the observed luminosities. If true, the measured luminosity of a particular star would only indicate a crude age, while the average distribution of stars in a cluster should still reflect the age of the cluster and act as an empirical isochrone. Thus, a comparison of GG Tau to the locus of stars in IC 348 can test both the coevality of the multiple system and the precision with which luminosities trace age. As illustrated in Figs. 8 and 9, the components of GG Tau form a line parallel to the population in IC 348. If the observed luminosities of young stars were dominated by factors other than age, the components of GG Tau should have luminosities randomly drawn from the range of values found in young clusters, and this is clearly not the case. Hence, it is indeed likely that the luminosities do reflect the age of GG Tau and that the components are coeval.

For each set of models, I will examine if the inferred age for GG Tau and average age and age spread for IC 348 are constant as a function of mass, whether a temperature scale intermediate between those of dwarfs and giants can improve agreement, and review other observational constraints discussed by LR98, Luhman (1998), and W99. The sample in IC 348 is representative down to M5-M6 and biased towards less reddened and more luminous objects at later types. Consequently, for stars earlier than M6, the average and upper and lower boundaries of the locus can be compared directly to the model isochrones. Later than M6, the upper envelope should be representative, and the average locus and lower envelope can be treated as upper limits.

### 3.5.3. D'Antona & Mazzitelli 1997

The models of DM97 are fairly consistent with the stellar parameters derived for the eclipsing binaries CM Dra ( $0.22 M_{\odot}$ ) and YY Gem ( $0.6 M_{\odot}$ ). The predicted radii agree with the values measured for CM Dra while different by two sigma from those of YY Gem (see Luhman 1998). The temperatures and luminosities are within two sigma and one sigma of the measurements for CM Dra and YY Gem, respectively. As seen in Figure 8, when the Pleiades brown dwarfs Teide 1 and Calar 3 are placed on the H-R diagram with the dwarf temperature scale, the age inferred from DM97 agrees with the age of the Pleiades (125 Myr; Stauffer, Schultz & Kirkpatrick 1998). The models are also consistent with the masses ( $65 M_J$ ; Basri & Martín 1998) and ages of the binary components of PPL 15. An additional test of the models is provided by the dynamical

mass measured for the system of GG Tau Aa and Ab through observations of the circumbinary disk ( $1.28 \pm 0.08 M_{\odot}$ ; Dutrey, Guilloteau, & Simon 1994; Guilloteau, Dutrey, & Simon 1999). Similar estimates are available for GM Aur ( $0.84 \pm 0.05 M_{\odot}$ ; Dutrey et al. 1998) and DM Tau ( $0.47 \pm 0.06 M_{\odot}$ ; Guilloteau & Dutrey 1998). For DM97, W99 found that the inferred masses of GG Tau A ( $0.80 M_{\odot}$ ) and GM Aur ( $0.51 M_{\odot}$ ) are lower than the observed values, while the predicted mass of DM Tau ( $0.44 M_{\odot}$ ) is consistent with the data. However, because of the uncertainty in the inclination of GM Aur, Dutrey et al. (1998) cannot rule out a mass of  $0.6 M_{\odot}$ , which is close to the mass implied by DM97.

The H-R diagram in Figure 8 indicates that the average age and age spread for IC 348 with the models of DM97 is fairly constant as a function of mass, except at  $0.05$ - $0.15 M_{\odot}$  where the isochrones rise relative to the observed locus. The same trend is seen for GG Tau. The components Aa, Ab, and Bb are coeval on the model isochrones while Ba is older. The only change in the temperature scale that could produce agreement between the empirical and theoretical isochrones is adjusting spectral types of M4-M6 to cooler temperatures without changing the scale at other types. Such a conversion would be discontinuous and cooler than the scales of dwarfs and giants and therefore is not a reasonable option. The models of DM97 are most compatible with the dwarf temperature scale adopted in this work, supporting the accuracy of the IMFs derived in previous studies of LRLL and Luhman & Rieke (1999) that used this combination of tracks and temperature scale. However, DM97 may underestimate masses above  $0.5 M_{\odot}$ , possibly introducing a systematic error in the IMFs at intermediate masses.

### 3.5.4. *Burrows et al. 1997*

Since the models of Burrows et al. (1997) include only masses of  $\leq 0.1 M_{\odot}$ , they cannot be tested directly against the data for CM Dra and YY Gem or the dynamical mass estimates of GG Tau A, DM Tau, and GM Aur. Model X of Burrows et al. (1993) reproduces the radii of the CM Dra components but predicts temperatures and luminosities that fall outside of the uncertainties of the measurements by two and three sigma, respectively (Luhman 1998). At  $0.1 M_{\odot}$ , the radius, temperature, and luminosity at the main sequence calculated by Burrows et al. (1997) are very similar to the values predicted in Model X, thus the newer models probably do not agree with the data for CM Dra either. As with DM97, the calculations of Burrows et al. (1997) are consistent with the data for the Pleiades brown dwarfs. Given the limited range of masses calculated by Burrows et al. (1997), a comparison of the theoretical isochrones to the locus in IC 348 and GG Tau is not conclusive. The models imply that most of the objects in IC 348 have ages less than 1 Myr, much younger than expected from other evidence, such as the fraction of sources exhibiting IR excess emission (LRLL; Lada & Lada 1995). There is also a tendency towards younger ages at higher masses in Figure 8, and no temperature scale between dwarfs and giants removes this implied age gradient.

### 3.5.5. Baraffe *et al.* 1998

The radius, temperature, and luminosity as a function of mass predicted by B98 for a main sequence star closely matches the calculations of DM97 above  $0.2 M_{\odot}$ . Thus, the comparison of DM97 to the data for CM Dra and YY Gem applies to B98 as well. In the H-R diagram in Figure 9, the 100 Myr isochrone of B98 is within the uncertainties of data for the Pleiades brown dwarfs Teide 1 and Calar 3. However, if PPL 15 is an equal mass binary, then the system luminosity shown in the H-R diagram should be reduced by 0.3 dex to reflect the individual components. At this new position PPL 15, falls below the 100 Myr isochrone and above the hydrogen burning limit, which is not consistent with the age of the Pleiades or the substellar mass of 65-80  $M_J$  implied by the binary data (Basri & Martín 1998) and Li measurements (Basri, Marcy, & Graham 1996).

The theoretical PMS evolution of stars at intermediate masses ( $> 0.6 M_{\odot}$ ) is sensitive to the treatment of convection (Chabrier & Baraffe 1997). Before the study of B98 was published, models with a mixing length parameter of  $\alpha = 1.0$  were made available for use in the work of LR98, LLR, Luhman (1998), and Luhman *et al.* (1998a). B98 subsequently concluded that calculations with  $\alpha = 1.9$  reproduced the properties of the Sun. Compared to the observed masses of  $1.28 \pm 0.08 M_{\odot}$ ,  $0.6$ - $0.9 M_{\odot}$ , and  $0.47 \pm 0.06 M_{\odot}$  for GG Tau A, GM Aur, and DM Tau, W99 derived B98 masses of 2.00, 1.06, and  $0.67 M_{\odot}$  for  $\alpha = 1.0$  and 1.46, 0.78, and  $0.64 M_{\odot}$  for  $\alpha = 1.9$ . Not only do the models with  $\alpha = 1.0$  fail to work for the Sun, but they also significantly overestimate masses in young solar-mass stars, which was indicated previously by LR98 and Luhman (1998) in examining the IMF of L1495E. On the other hand, the calculations with  $\alpha = 1.9$  produce fairly good agreement with the data for solar-mass stars at both the main sequence and the earliest stages.

The data for IC 348 and GG Tau are shown with the models of B98 ( $\alpha = 1.9$ ) in Figure 9. The isochrones imply an age gradient in both sets of data, where the less massive objects are progressively younger. W99 suggested that a warmer temperature scale for GG Tau Ba and Bb could bring them onto the same model isochrone as Aa and Ab. The necessary departure from a dwarf scale is increased slightly by the revision of Ba and Bb to later spectral types (§ 3.2.2). The temperatures of Ba and Bb that are required for coevality are shown in Figure 7. These temperatures are reasonable for PMS objects since they are intermediate between dwarf and giant values. The warmer source Ba is closer to the dwarf scale than Bb. As an experiment, this trend is extrapolated to earlier types until M0, where the dwarf and giant scales converge. For M8 and M9, the temperatures were selected to be continuous with the values at earlier types and intermediate between dwarfs and giants with no other justification. This intermediate temperature scale is listed in Table 2 and illustrated in Figure 7. Using this scale, the data for GG Tau and IC 348 are placed on the H-R diagram in the lower panel of Figure 9. As defined, the components of GG Tau are now coeval on the isochrones of B98. In addition, the locus of IC 348 maintains a constant age and age spread with mass on these isochrones. Although construction of the intermediate temperature scale was somewhat ad hoc at types earlier and later than GG Tau Ba and Bb, using this scale with the B98 models is consistent with the constraints at young ages over a wide range

of masses, and should therefore provide the relatively reliable ages and masses.

### 3.5.6. Implications of Tests

The theoretical calculations of the evolution of low-mass stars and brown dwarfs have become quite sophisticated in recent years. However, among the various models there remain large differences in the predicted path of these objects on the H-R diagram, particularly at ages of  $< 10$  Myr. Consequently, the masses and ages estimated for young low-mass objects are sensitive to the choice of models and the adopted a temperature scale. Given the observational constraints provided GG Tau and IC 348, the models of DM97 are compatible with the dwarf temperature scale, while a scale intermediate between those of dwarfs and giants works well with B98. The calculations of Burrows et al. (1997) do not appear to provide an adequate description of young low-mass sources for any reasonable temperature scale. Both models of B98 and DM97 imply that the hydrogen burning limit at young ages occurs at a spectral type of  $\sim$ M6 and that several objects in IC 348 fall below the substellar boundary with masses as low as 20-30  $M_J$ .

## 4. Conclusion

I have obtained deep optical photometry and spectroscopy of the young cluster IC 348 and combined it with previous IR and optical observations. The conclusions are as follows:

1. Expanding on previous optical and IR searches for low-mass stars and brown dwarfs in IC 348, I have identified a rich population of new low-mass candidates through  $R$  and  $I$  photometry. Low-resolution optical spectroscopy of a subset of these objects has confirmed their youth and late spectral types.
2. Using the large number of sources in the spectroscopic sample, I have described the typical behavior of the optical spectra of young late-type objects (M5-M8.5) relative to standard dwarfs and giants. Overall, averages of dwarf and giant spectra closely resemble the optical data for young objects and comprise good calibrators of spectral types for young low-mass populations.
3. It appears that the intrinsic  $R - I$  and  $I - J$  colors of young late M objects are intermediate between the colors of dwarfs and giants, which is consistent with the behavior of the spectra in these bands. Meanwhile, the intrinsic  $J - H$  and  $H - K$  colors are dwarf-like with an additional  $H - K$  excess in some sources, probably arising from a circumstellar disk or an infalling envelope.
4. After testing the models with empirical isochrones in the form of the multiple system GG Tau and the population of IC 348, I find that the calculations of Burrows et al. (1997)

are not consistent with the data while the models of DM97 are roughly compatible with the data when a dwarf temperature scale is used. The models of B98 produce the best agreement with observational constraints at young ages, particularly if a temperature scale intermediate between those of dwarfs and giants is adopted.

5. Under the constraints of the empirical isochrones, both DM97 and B98 suggest that the hydrogen burning limit occurs near M6 at ages of  $\lesssim 10$  Myr. These models indicate the presence of several new brown dwarfs in the spectroscopic sample of IC 348.

I am particularly grateful to the staff of Keck Observatory for their careful execution of the service observations. I thank F. Allard, I. Baraffe, A. Burrows, N. Calvet, and F. D'Antona for providing their most recent calculations and useful advice. Comments on the manuscript by L. Hartmann, G. Rieke, J. Stauffer, and R. White are greatly appreciated. I also thank R. White for access to his spectra of GG Tau B. I was funded by a postdoctoral fellowship at the Harvard-Smithsonian Center for Astrophysics. Some of the data presented herein were obtained at the W. M. Keck Observatory, which is operated as a scientific partnership among the California Institute of Technology, the University of California, and the National Aeronautics and Space Administration. The Observatory was made possible by the generous financial support of the W. M. Keck Foundation.

## REFERENCES

Baraffe, I., Chabrier, G., Allard, F., & Hauschildt, P. H. 1998, *A&A*, 337, 403 (B98)  
Basri, G., Marcy, G. W., & Graham, J. R. 1996, *ApJ*, 458, 600  
Basri, G., & Martín, E. L. 1998, in *ASP Conf. Ser.* 134, *Brown Dwarfs and Extrasolar Planets Proceedings*, ed. R. Rebolo, E. L. Martín, M. R. Zapatero-Osorio (San Francisco: ASP), 284  
Béjar, V. J. S., Zapatero Osorio, M. R., & Rebolo, R. 1999, *ApJ*, in press  
Bessell, M. S. 1991, *AJ*, 101, 662  
Bessell, M. S., & Brett, J. M. 1988, *PASP*, 100, 1134  
Briceño, C., Hartmann, L., Stauffer, J., & Martín, E. L., 1998, *AJ*, 115, 2074  
Burrows, A., Hubbard, W. B., Saumon, D., & Lunine, J. I. 1993, *ApJ*, 406, 158  
Burrows, A., Marley, M., Hubbard, W. B., Lunine, J. I., Guillot, T., Saumon, D., Freedman, R., Sudarsky, D., & Sharp, C. 1997, *ApJ*, 491, 856  
Chabrier, G., & Baraffe, I. 1997, *A&A*, 327, 1039  
Comerón, F., Rieke, G. H., & Neuhäuser, R. 1999, *A&A*, 343, 477

D'Antona, F., & Mazzitelli, I. 1997, in “Cool stars in Clusters and Associations”, eds. R. Pallavicini & G. Micela, Mem.S.A.It., 68, n.4 (DM97)

Delfosse, X., et al. 1997, A&A, 327, L25

Dutrey, A., Guilloteau, S., Prato, L., Simon, M., Duvert, G., Schuster, K., & Menard, F. 1998, A&A, 338, 63

Dutrey, A., Guilloteau, S., & Simon, M. 1994, A&A, 286, 149

Ghez, A. M., White, R. J., & Simon, M. 1997, ApJ, 490, 353

Guilloteau, S., & Dutrey, A. 1998, A&A, 339, 467

Guilloteau, S., Dutrey, A., & Simon M. 1999, submitted

Gullbring, E., Hartmann, L., Briceño, C., & Calvet, N. 1998, ApJ, 492, 323

Hartigan, P., Strom, K. M., & Strom, S. E. 1994, ApJ, 427, 961

Henry, T. J., Kirkpatrick, J. D., & Simons, D. A. 1994, AJ, 108, 1437

Herbig, G. H. 1998, ApJ, 497, 736

Hillenbrand, L. A. 1997, AJ, 113, 1733

Kenyon, S. J., & Hartmann, L. 1995, ApJS, 101, 117

Kirkpatrick, J. D., et al. 1999, ApJ, 519, ???

Kirkpatrick, J. D., Henry, T. J., & Irwin, M. J. 1997, AJ, 113, 1421

Kirkpatrick, J. D., Henry, T. J., & McCarthy, D. W. 1991, ApJS, 77, 417

Kirkpatrick, J. D., Kelly, D. M., Rieke, G. H., & Liebert, J. 1993, ApJ, 402, 643

Lada, E. A., & Lada, C. J. 1995, AJ, 109, 1682

Landolt, A. U. 1992, AJ, 104, 340

Leggett, S. K. 1992, ApJS, 82, 351

Leggett, S. K., Allard, F., Berriman, G., Dahn, C. C., & Hauschildt, P. H. 1996, ApJS, 104, 117

Leggett, S. K., Allard, F., & Hauschildt, P. H. 1998, ApJ, 509, 836

Lowrance, P. J., et al. 1999, ApJ, 512, L69

Luhman, K. L. 1998, in ASP Conf. Ser. 134, Brown Dwarfs and Extrasolar Planets Proceedings, ed. R. Rebolo, E. L. Martín, M. R. Zapatero-Osorio (San Francisco: ASP), 532

Luhman, K. L., Briceño, C., Rieke, G. H., & Hartmann, L. W. 1998a, ApJ, 493, 909

Luhman, K. L., Liebert, J., & Rieke, G. H. 1997, ApJ, 489, L165 (LLR)

Luhman, K. L., & Rieke, G. H. 1998, ApJ, 497, 354 (LR98)

Luhman, K. L., & Rieke, G. H. 1999, ApJ, in press

Luhman, K. L., Rieke, G. H., Lada, C. J., & Lada, E. A. 1998b, ApJ, 508, 347 (LRLL)

Martín, E. L., Basri, G., Delfosse, X., & Forveille, T. 1997, *A&A*, 327, L29

Martín, E. L., Basri, G., Zapatero Osorio, M. R., Rebolo, R., & García López, R. J. 1998, *ApJ*, 507, L41

Meyer, M. R., Calvet, N., & Hillenbrand, L. A. 1997, *AJ*, 114, 288

Monet, D. G., Dahn, C. C., Vrba, F. J., Harris H. C., Pier, J. R., Luginbuhl, C. B., & Ables, H. D. 1992, *AJ*, 103, 638

Nakajima, T., Oppenheimer, B. R., Kulkarni, S. R., Golimowski, D. A., Matthews, K., & Durrance, S. T. 1995, *Nature*, 378, 463

Oke, J. B., et al. 1995, *PASP*, 107, 375

Oppenheimer, B. R., Kulkarni, S. R., Nakajima, T., & Matthews, K. 1995, *Science*, 270, 1478

Perrin, G., Coudé du Foresto, V., Ridgway, S. T., Mariotti, J.-M., Traub, W. A., Carleton, N. P., & Lacasse, M. G. 1998, *A&A*, 331, 619

Prato, L. A. 1998, Ph. D. thesis, State Univ. of New York at Stony Brook

Rebolo, R., Zapatero Osorio, M. R., Madruga, S., Béjar, V. J. S., Arribas, S., & Licandro, J. 1998, *Science*, 282, 1309

Reid, I. N., & Hawley, S. L. 1999, *ApJ*, 117, 343

Rieke, G. H., & Lebofsky, M. J. 1985, *ApJ*, 288, 618

Richichi, Ragland, S., Stecklum, B., & Leinert, C. 1998, *A&A*, 338, 527

Ruiz, M. T., Leggett, S. K., & Allard, F. 1997, *ApJ*, 491, L107

Stauffer, J. R., Hamilton, D., & Probst, R. G. 1994, *AJ*, 108, 155

Stauffer, J. R., Hartmann, L. W., & Barrado, D. 1995, *ApJ*, 454, 910

Stauffer, J. R., Schultz, G., & Kirkpatrick, J. D. 1998, *ApJ*, 499, 199

Strom, K. M., & Strom, S. E. 1994, *ApJ*, 424, 237

Tinney, C. G., Delfosse, X., & Forveille, T. 1997, *ApJ*, 490, L95

Tinney, C. G., Mould, J. R., & Reid, I. N. 1993, *AJ*, 105, 1045

Trullols, E. & Jordi, C. 1997, *A&A*, 324, 549

van Belle, G. T., et al. 1999, *ApJ*, 117, 521

White, R. J., Ghez, A. M., Reid, I. N., & Schultz, G. 1999, *ApJ*, in press (W99)

Wilking, B. A., Greene, T. P., & Meyer, M. R. 1998, *AJ*, 117, 469

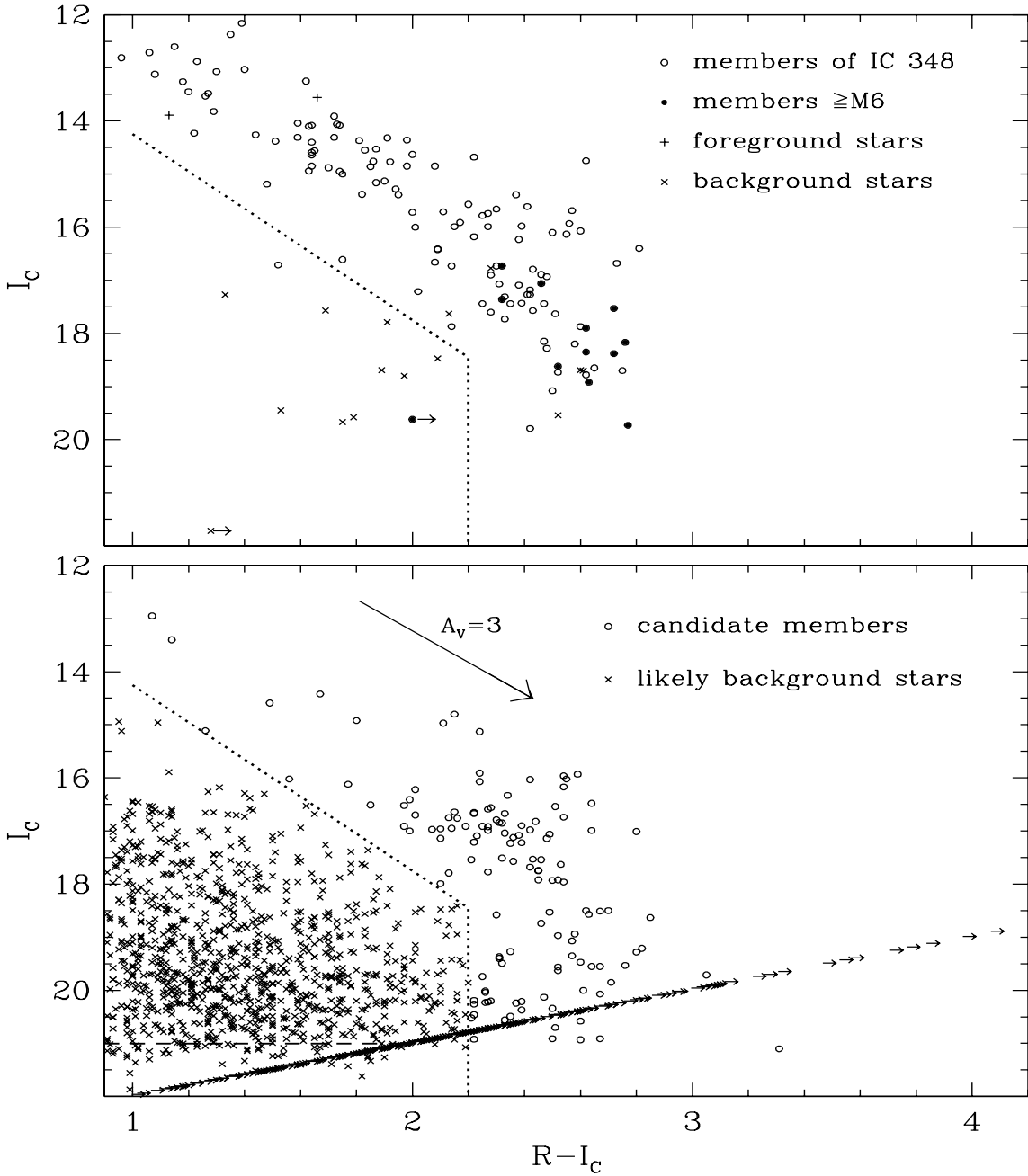


Fig. 1.—  $R - I$  vs.  $I$  for an area of  $25' \times 25'$  towards IC 348. The spectroscopic sample is given in the upper panel, where cluster members, likely substellar members ( $\geq M6$ ), and field stars are indicated. The lower panel shows the remaining stars that have not been observed spectroscopically. For sources that are saturated in my data ( $I \lesssim 16.5$ ), measurements of Herbig (1998) are used for the central  $7' \times 14'$  of the cluster. Completeness limits of  $I \sim 21$  and  $R \sim 23$  are indicated by the dashed line and arrows.

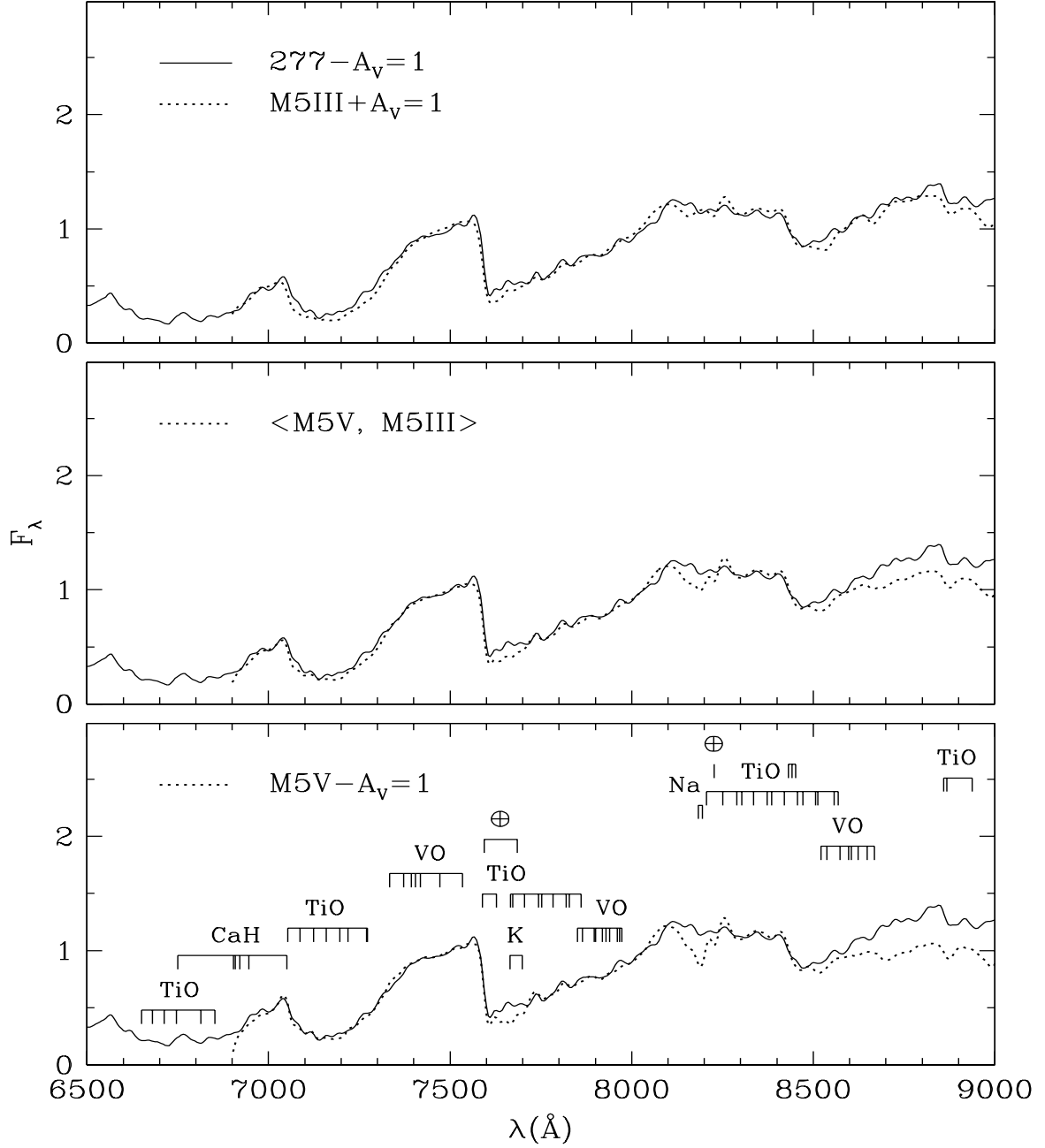


Fig. 2.— The spectrum of object 277, dereddened by  $A_V = 1$  to approximate the intrinsic spectrum (see § 3.2.2), is shown with data for M5V, M5III, and an average of the two. For easier comparison of the spectral features, the slopes have been matched by adjusting the reddening of the standards. The young object’s intrinsic spectrum is bluer than M5V, hence a negative extinction must be applied to the standard to produce a match. All data are smoothed to a resolution of 25  $\text{\AA}$  and normalized at 7500  $\text{\AA}$ .

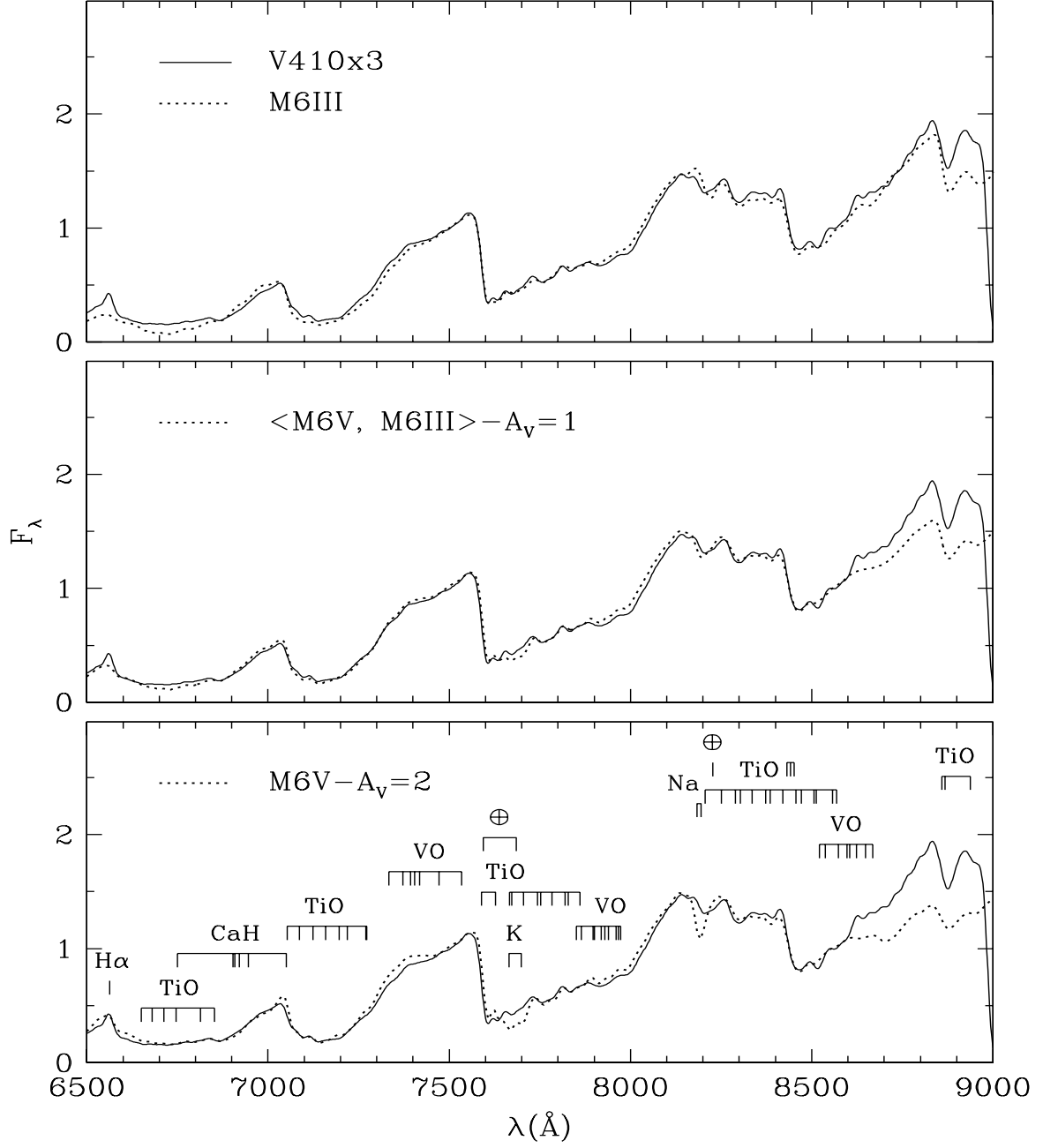


Fig. 3.— The spectrum of V410 X-ray 3 (Luhman et al. 1998a), dereddened by  $A_V = 0.6$  to approximate the intrinsic spectrum (see § 3.2.2), is shown with data for M6V, M6III, and an average of the two. For easier comparison of the spectral features, the slopes have been matched by adjusting the reddenings of the standards. The young object’s intrinsic spectrum is bluer than M6V and an average of M6V and M6III, hence a negative extinction must be applied to the standard to produce a match. All data are smoothed to a resolution of 25  $\text{\AA}$  and normalized at 7500  $\text{\AA}$ .

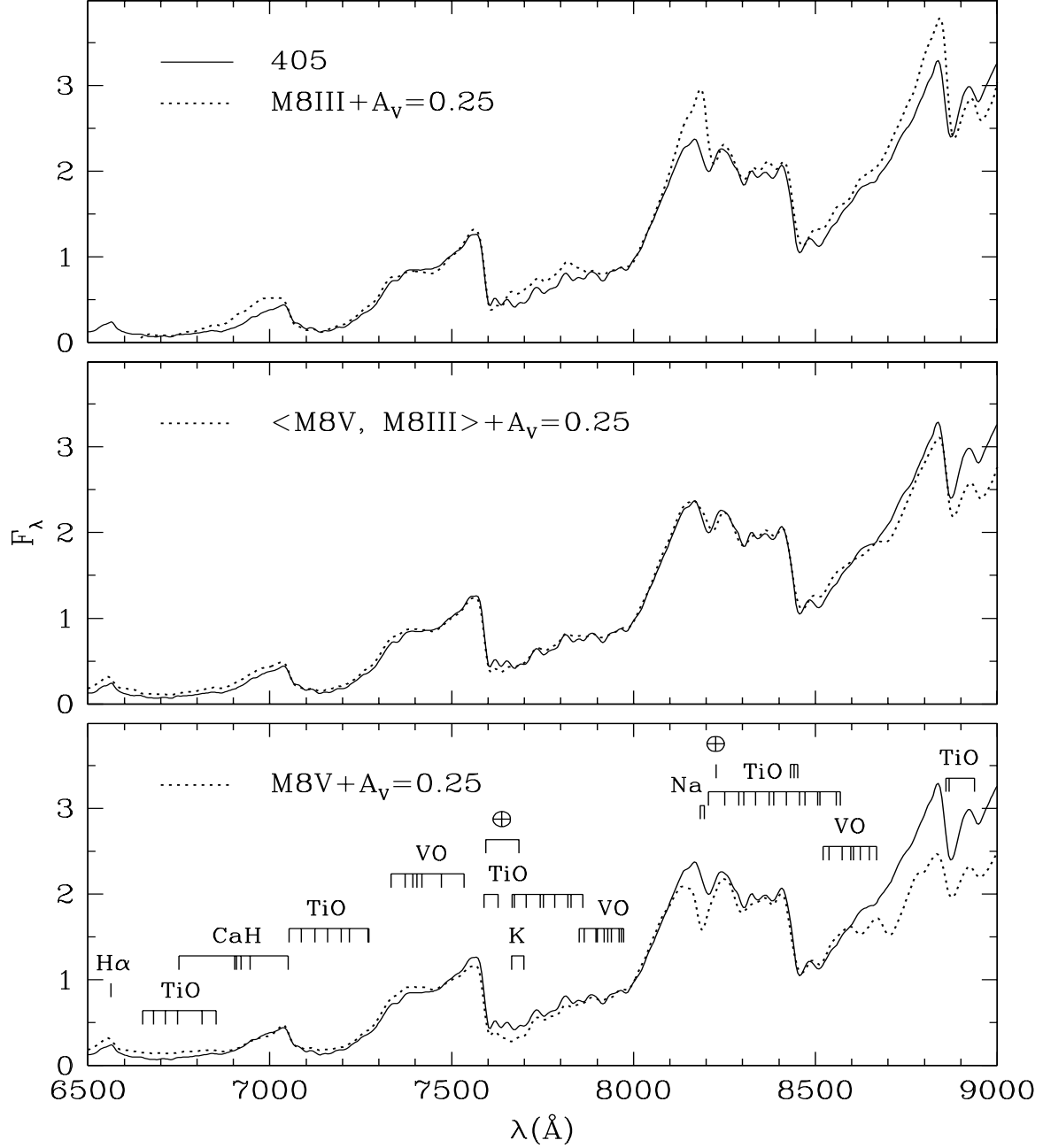


Fig. 4.— The standard spectra of M8V, M8III, and an average of the two are reddened slightly ( $A_V = 0.25$ ) to match the data for source 405. All data are smoothed to a resolution of 25  $\text{\AA}$  and normalized at 7500  $\text{\AA}$ .

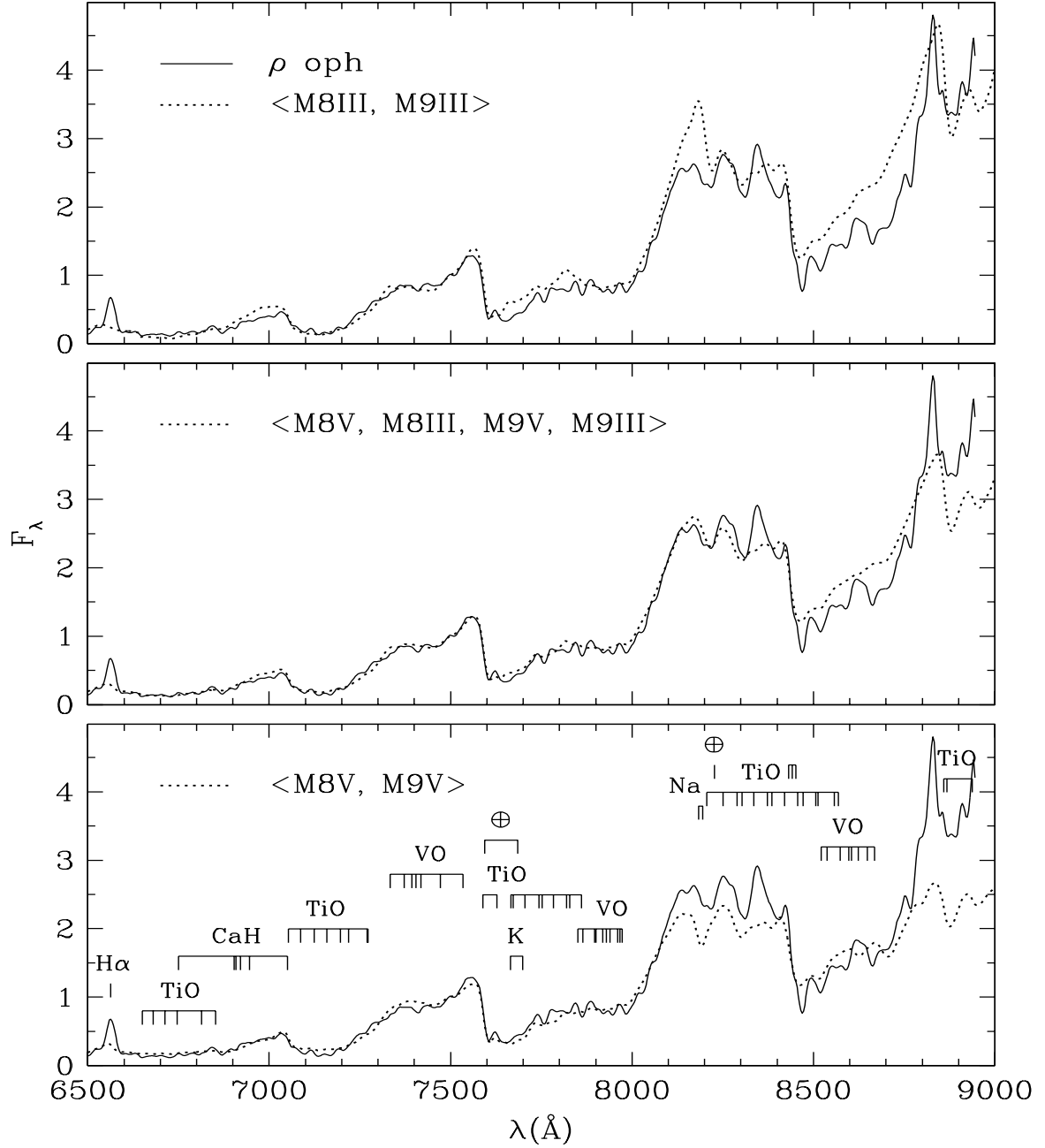


Fig. 5.— The spectrum ( $A_V < 0.7$ ) of the  $\rho$  Oph brown dwarf GY141 is shown with data for standard M8 and M9 dwarfs and giants. All data are smoothed to a resolution of 25  $\text{\AA}$  and normalized at 7500  $\text{\AA}$ .

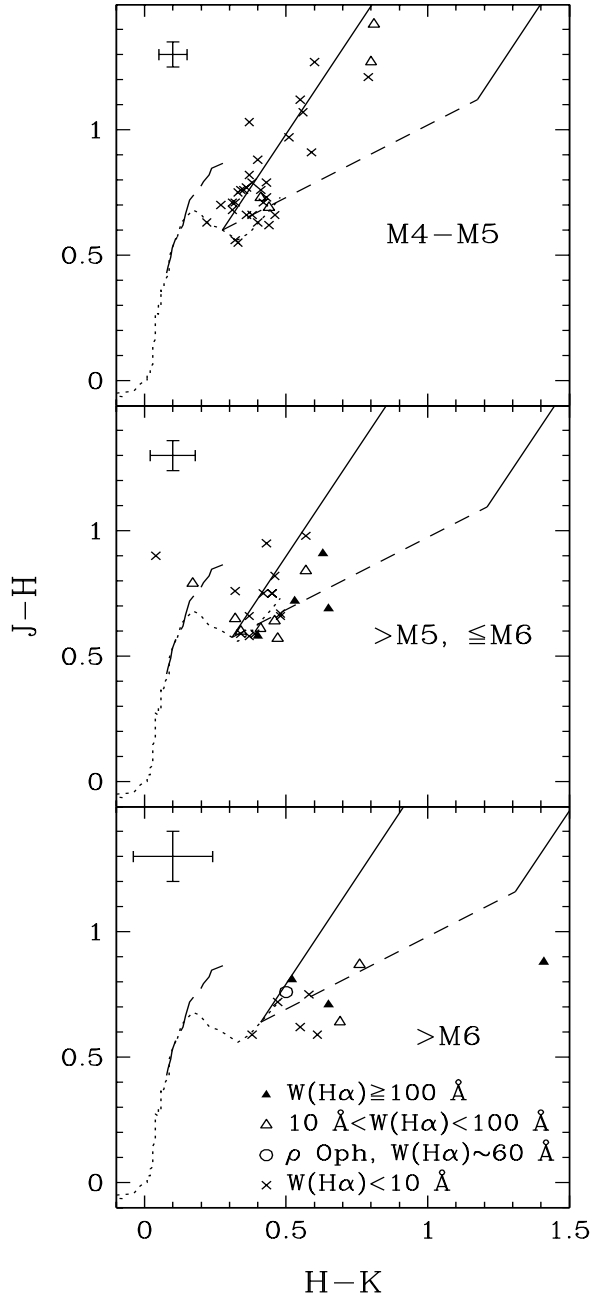


Fig. 6.—  $H - K$  vs.  $J - H$  for late-type members of IC 348 and the  $\rho$  Oph brown dwarf GY141 sorted by spectral type and  $H\alpha$  strength and shown with typical colors of field dwarfs (dotted line;  $\leq M9$ ) and giants (long dashed line;  $\leq M5$ ). The locus of classical T Tauri stars ( $\sim M0$ ) measured by Meyer, Hillenbrand, & Calvet (1997) (short dashed line) and reddening vectors (solid lines) are plotted with the origin placed at the dwarf colors of each spectral type. The error bars represent the typical uncertainties in the colors from Lada & Lada (1995). More accurate colors from LRLL have been used when available.

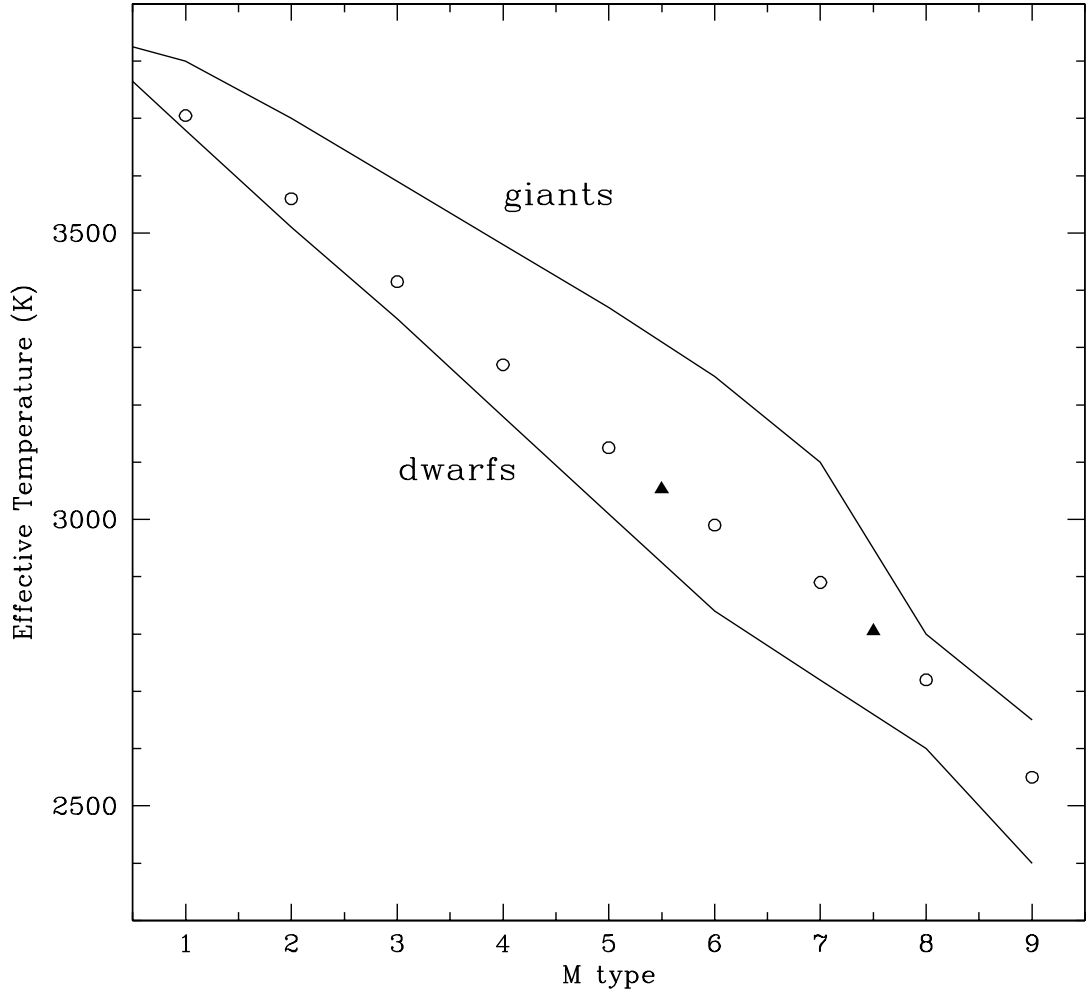


Fig. 7.— The temperature scales for cool dwarfs (Leggett et al. 1996; see text) and giants (Perrin et al. 1998; Richichi et al. 1998; van Belle et al. 1999) listed in Table 2. If the four components of GG Tau are coeval, then the models of B98 imply temperatures for GG Tau Ba and Bb (solid triangles) that are between dwarf and giant values. An intermediate temperature scale that is consistent with these results has been constructed (open circles) and is used in the H-R diagram in the lower panel of Figure 9.

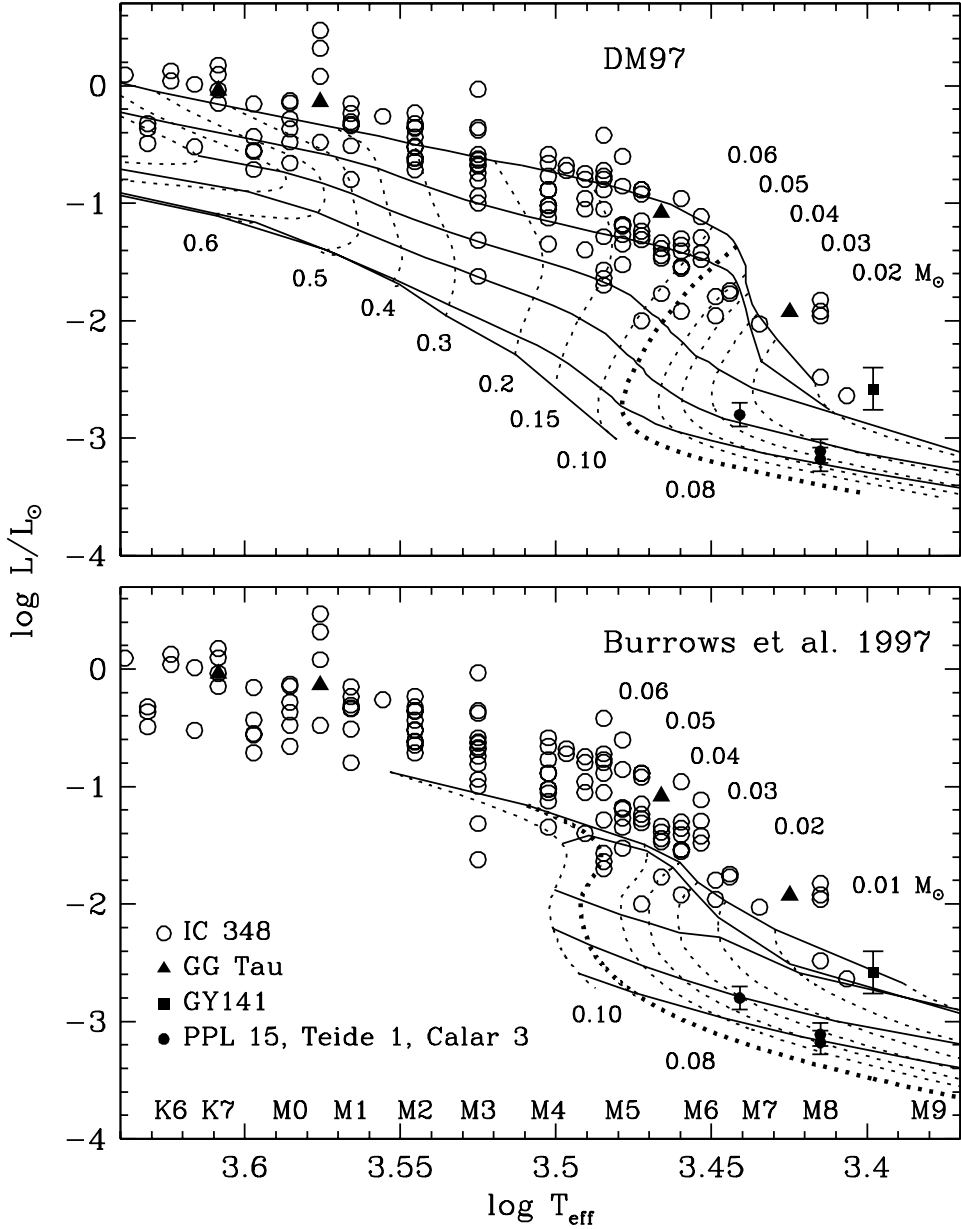


Fig. 8.— H-R diagram for all known late-type sources in IC 348 assuming a distance modulus of 7.5 with the evolutionary models of DM97 and Burrows et al. (1997), where the horizontal solid lines are isochrones representing ages of 1, 3, 10, 30, and 100 Myr and the main sequence, from top to bottom. The latter calculations differ from those of Burrows shown in LLR and LRLL (see text). The four components of the multiple system GG Tau (White et al. 1999) are expected to be coeval. The  $\rho$  Oph brown dwarf GY141 and the Pleiades brown dwarfs PPL 15, Teide 1, and Calar 3 are also given for reference. Spectral types have been converted to effective temperatures with a dwarf temperature scale. Uncertainties in spectral types are typically  $\pm 0.25$  subclass.

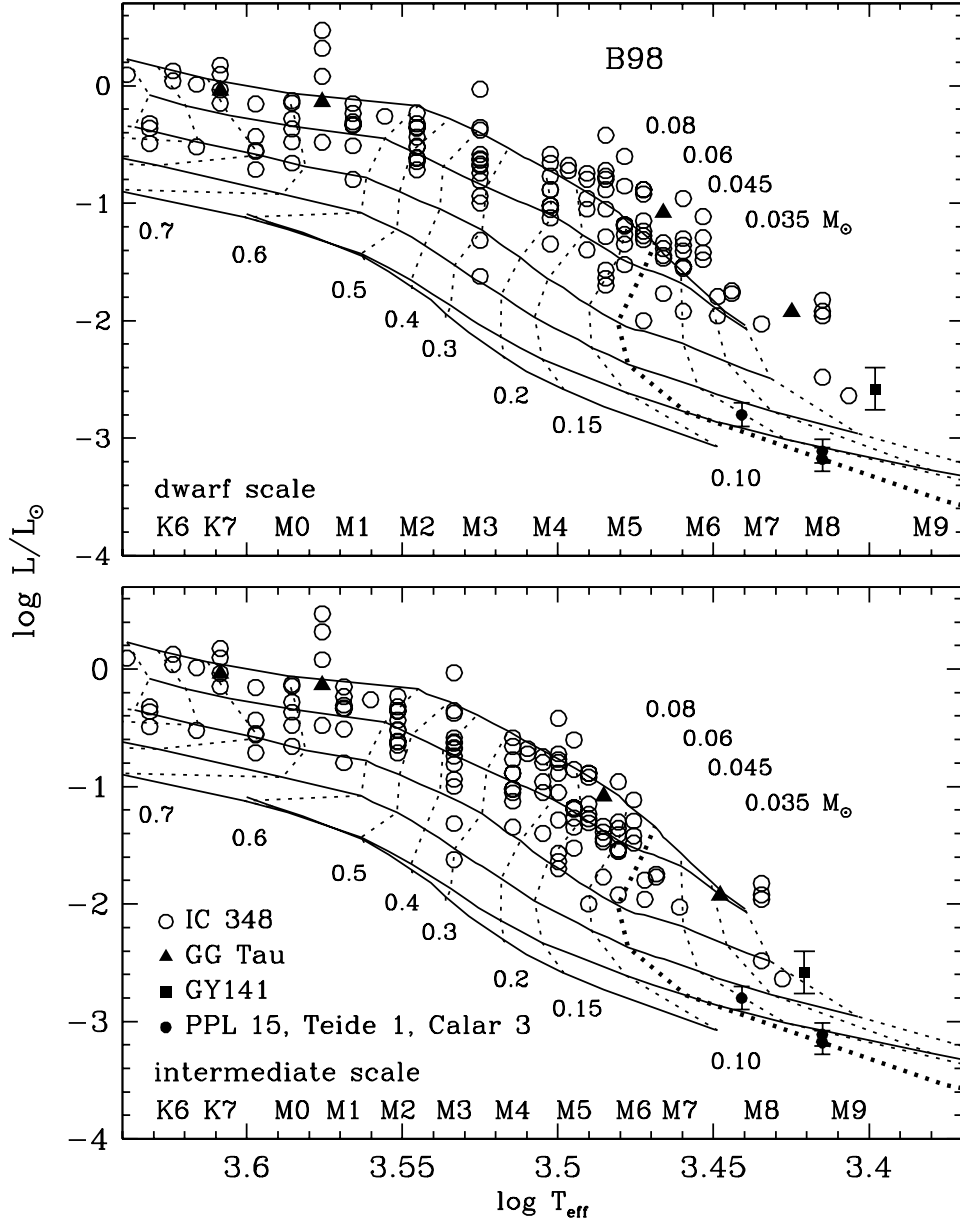


Fig. 9.— H-R diagram for all known late-type sources in IC 348 with the evolutionary models of B98, where the horizontal solid lines are isochrones representing ages of 1, 3, 10, 30, and 100 Myr and the main sequence, from top to bottom. In the upper panel, spectral types have been converted to effective temperatures with a dwarf temperature scale. In the lower panel, the data are plotted with a scale such that GG Tau Ba and Bb fall on the same model isochrone as Aa and Ab. This temperature scale is intermediate between those of dwarfs and giants, and is given in Table 2 and Figure 7. The Pleiades brown dwarfs PPL 15, Teide 1, and Calar 3 are plotted with a dwarf scale. Uncertainties in spectral types are typically  $\pm 0.25$  subclass.

Table 2. Temperature Scales

Spectral Type	$T_{\text{eff}}$ (K)		
	Dwarf <sup>a</sup>	Giant <sup>b</sup>	Intermediate <sup>c</sup>
M1	3680	3800	3705
M2	3510	3700	3560
M3	3350	3590	3415
M4	3180	3480	3270
M5	3010	3370	3125
M6	2840	3250	2990
M7	2720	3100	2890
M8	2600	2800	2720
M9	2400	2650	2550

<sup>a</sup>Leggett et al. 1996 with an extrapolation to types later than M6.5.

<sup>b</sup>Perrin et al. 1998; Richichi et al. 1998; van Belle et al. 1999.

<sup>c</sup>When this temperature scale is combined with the models of Baraffe et al. 1998, the four components of GG Tau are coeval.

TABLE 1  
DATA FOR LOW-MASS SOURCES IN IC 348

ID	$\alpha$ (2000)	$\delta$ (2000)	Spectral Type/ $W_\lambda$ (H $\alpha$ ) <sup>a</sup>	Adopt	$T_{\text{eff}}$ <sup>b</sup>	$A_J$	$L_{\text{bol}}$	$R - I$ H98	$I$	$R - I$ this work	$I$	$J - H$	$H - K$ LL	$K$	$J - H$	$H - K$ LRLL	$K$
42 <sup>c</sup>	3 44 42.05	32 08 58.40	M4-M6(IR),M3/74(H98)	M4	3180	0.32	0.088	1.87	15.16	...	...	1.07	0.72	10.20	...	...	...
62	3 44 26.51	32 03 58.4	M4.75/10	M4.75	3052	0.46	0.38	...	...	...	...	0.77	0.36	10.65	...	...	...
95	3 44 21.98	32 12 11.3	M2-M4(IR),M4/5.5(LRLL)	M4	3180	0.37	0.26	...	...	...	...	0.75	0.33	11.07	...	...	...
124	3 43 54.38	32 00 31.4	M4.25/7	M4.25	3138	0.41	0.19	...	...	...	...	0.76	0.41	11.32	...	...	...
130	3 44 04.29	32 13 50.2	>K5(IR),M4.75/5(LRLL)	M4.75	3052	0.43	0.19	...	...	...	...	0.76	0.34	11.38	...	...	...
133	3 44 41.81	32 12 00.6	M5-M6(IR),M4-M5(LRLL)	M5	3010	1.26	0.25	...	...	...	...	1.07	0.56	11.39	...	...	...
135	3 44 39.49	32 20 07.6	>K5(IR),M4.5/20(LRLL)	M4.5	3095	0.24	0.16	...	...	...	...	0.69	0.44	11.41	...	...	...
137	3 44 11.63	32 19 40.8	M4-M6(IR),M3-M4/8(LRLL)	M4	3180	0.26	0.17	...	...	...	...	0.71	0.32	11.45	...	...	...
145	3 44 41.38	32 10 22.9	M2-M4(IR),M4.75/4(LRLL)	M4.75	3052	0.28	0.17	2.22	14.68	...	...	0.70	0.27	11.51	...	...	...
150	3 45 02.84	32 06 56.6	M4.75/8	M4.75	3052	0.43	0.16	...	...	...	...	0.76	0.35	11.57	...	...	...
158	3 44 40.15	32 09 10.6	>K5(IR),M5(LRLL)	M5	3010	0.84	0.14	2.81	16.40	...	...	0.95	0.52	11.66	0.91	0.59	11.75
159	3 44 47.70	32 10 53.0	M4.25/4	M4.25	3138	1.36	0.21	2.73	16.68	...	...	1.12	0.55	11.68	...	...	...
160	3 44 02.31	32 01 35.3	M4.75/6	M4.75	3052	0.22	0.13	...	...	...	...	0.68	0.31	11.69	...	...	...
163	3 44 11.18	32 08 17.1	M5.25/10.5	M5.25	2968	0.18	0.13	2.62	14.75	...	...	0.65	0.32	11.74	...	...	...
165	3 44 35.43	32 08 54.4	>K5(IR),M5.25/74±5(LRLL)	M5.25	2968	0.68	0.13	2.60	16.07	...	...	0.81	0.50	11.77	0.84	0.57	11.74
169	3 44 17.61	32 04 47.3	K6-M1? <sup>c</sup> (IR),M5.25/7	M5.25	2968	0.44	0.12	2.57	15.69	...	...	0.75	0.45	11.81	...	...	...
173	3 44 09.98	32 04 05.4	M5.75/110±10	M5.75	2882	0.40	0.11	...	...	...	...	0.72	0.53	11.85	...	...	...
175	3 44 49.74	32 03 31.3	M4.5/8	M4.5	3095	0.34	0.11	...	...	...	...	0.73	0.43	11.86	...	...	...
184	3 44 53.72	32 06 48.7	M4/5	M4	3180	0.71	0.13	2.27	15.74	...	...	0.88	0.40	11.94	...	...	...
192	3 44 23.44	32 01 52.1	M4-M5/40±20	M4.5	3095	2.16	0.18	...	...	2.90	18.62	1.42	0.81	12.07	...	...	...
201	3 45 01.66	32 12 25.5	M4/5	M4	3180	0.26	0.095	...	...	...	...	0.71	0.31	12.12	...	...	...
205	3 44 29.54	32 00 53.2	M6/140±15	M6	2840	0.34	0.077	...	...	...	...	0.69	0.65	12.15	...	...	...
217	3 44 43.08	32 10 12.8	M4-M6(IR),M3/4(H98)	M4	3180	0.47	0.096	2.55	16.13	...	...	0.82	0.33	12.24	0.79	0.38	12.17
218	3 44 44.62	32 07 27.4	K6-M1? <sup>c</sup> (IR),M4/8(H98)	M4	3180	1.11	0.13	2.85	16.72	2.47	16.76	0.98	0.51	12.24	1.03	0.37	12.26
223	3 44 41.54	32 13 07.4	M5/5	M5	3010	0.11	0.065	...	...	...	...	0.63	0.40	12.29	...	...	...
224	3 44 55.38	32 09 31.1	M4.75/7.5	M4.75	3052	0.59	0.089	...	...	...	...	0.82	0.37	12.30	...	...	...
229	3 44 57.76	32 03 58.0	M5.25/4.5	M5.25	2968	0.20	0.071	...	...	...	...	0.66	0.37	12.32	...	...	...
237	3 44 23.53	32 09 32.8	M4-M6? <sup>c</sup> (IR),M5/7(LRLL)	M5	3010	0.32	0.066	2.30	15.66	...	...	0.65	0.34	12.37	0.71	0.42	12.39
240	3 44 51.97	32 04 43.3	M3.5-M4.5	M4	3180	0.47	0.075	2.15	15.99	...	...	0.79	0.43	12.38	...	...	...
242	3 44 32.62	32 04 11.9	M5/30±15	M5	3010	0.37	0.066	...	...	...	...	0.73	0.41	12.43	...	...	...
256	3 43 55.14	32 07 55.0	M5.75/34	M5.75	2882	0.01	0.050	2.56	15.93	...	...	0.57	0.47	12.55	...	...	...
259	3 44 03.44	32 02 34.5	M4.5-M6	M5.25	2968	0.02	0.053	...	...	...	...	0.59	0.34	12.56	...	...	...
266	3 44 18.17	32 07 32.5	M4.75/4.5	M4.75	3052	0.17	0.052	2.27	15.99	...	...	0.66	0.36	12.63	...	...	...
277	3 44 39.47	32 10 05.9	M5/5	M5	3010	0.08	0.045	2.22	16.18	...	...	0.62	0.34	12.74	0.62	0.44	12.63
285	3 44 31.92	32 12 42.8	M4-M5	M4.5	3095	1.76	0.089	...	...	2.65	18.16	1.27	0.60	12.80	...	...	...
286	3 45 06.80	32 09 26.8	M5.75/6	M5.75	2882	0.03	0.044	...	...	...	...	0.58	0.37	12.81	...	...	...
287	3 44 41.08	32 08 05.0	M5-M5.5(LRLL)	M5.25	2968	1.05	0.058	3.00	17.89	2.66	17.84	0.97	0.60	12.81	0.98	0.57	12.87
292	3 43 59.73	32 04 42.5	M4.5-M6.5	M5.5	2925	0.22	0.041	2.66	16.71	2.31	16.73	0.66	0.48	12.86	...	...	...
294	3 44 24.54	32 10 02.1	M4.5(LRLL)	M4.5	3095	0.16	0.040	2.09	16.42	...	...	0.66	0.38	12.89	...	...	13.18
295	3 44 29.38	32 04 03.1	M5-M5.5/10?	M5.25	2968	0.63	0.049	...	...	2.39	17.09	0.82	0.46	12.89	...	...	...
301	3 44 22.49	32 01 41.8	M4.5-M5.5/30?	M5	3010	1.79	0.064	...	...	2.73	18.61	1.27	0.80	12.95	...	...	...
312	3 43 54.98	32 07 15.7	M6	M6	2840	0.53	0.051	2.74	16.67	2.34	16.73	0.76	0.32	13.04	...	...	...
314	3 44 22.35	32 01 27.2	M4.5-M5.5	M5	3010	1.63	0.054	...	...	2.69	18.74	1.21	0.79	13.05	...	...	...
319	3 45 01.15	32 12 19.1	M5.5/16	M5.5	2925	0.07	0.034	...	...	...	...	0.60	0.34	13.12	...	...	...
322	3 44 19.39	32 02 24.5	M4/9	M4	3180	0.95	0.045	...	...	2.25	17.43	0.97	0.51	13.16	...	...	...
324	3 44 45.27	32 10 53.5	M5.5-M6(LRLL)	M5.75	2882	0.48	0.039	2.64	17.18	2.34	17.31	0.63	0.42	13.20	0.75	0.42	13.16
325	3 44 30.02	32 08 47.3	M6(LRLL)	M6	2840	0.50	0.038	2.80	17.47	2.82	17.49	0.83	0.49	13.20	0.75	0.45	13.21
334	3 44 26.48	32 02 35.4	M5.75/27	M5.75	2882	0.19	0.029	...	...	2.27	16.91	0.64	0.46	13.27	...	...	...
335	3 44 44.24	32 08 44.6	M5.75/6(LRLL)	M5.75	2882	0.27	0.029	2.81	17.23	2.45	17.26	0.95	0.43	13.27	0.67	0.48	13.29
336	3 44 32.22	32 03 25.9	M5-M6/200±50	M5.5	2925	0.88	0.036	...	...	2.27	17.61	0.91	0.63	13.27	...	...	...
344	3 45 00.66	32 08 15.7	M4.5-M5.5/6	M5	3010	0.11	0.030	...	...	...	...	0.63	0.22	13.33	...	...	...
351	3 44 25.71	32 09 04.7	M5.5(LRLL)	M5.5	2925	0.99	0.046	2.75	17.61	2.45	17.56	0.79	0.39	13.36	0.95	0.43	13.27
353	3 44 38.18	32 10 19.3	M6/2(LRLL)	M6	2840	0.13	0.033	2.61	16.96	2.50	17.05	0.58	0.35	13.38	0.61	0.41	13.17
355	3 44 39.18	32 08 11.4	M8(LRLL)	M8	2600	0.08	0.015	3.12	18.12	2.79	18.18	0.65	0.61	13.42	0.72	0.47	13.46
360	3 44 43.79	32 10 45.6	M4.75/9(LRLL)	M4.75	3052	0.00	0.023	2.09	16.41	...	...	0.68	0.24	13.49	0.56	0.32	13.47
363	3 44 17.00	32 00 15.3	M8/12	M8	2600	0.00	0.012	...	...	2.56	17.95	0.64	0.69	13.50	...	...	...
366	3 44 35.03	32 08 55.3	M4.75/5(LRLL)	M4.75	3052	0.17	0.020	2.41	17.27	...	...	0.57	0.14	13.51	0.66	0.46	13.57
367	3 43 59.03	32 05 57.9	M6-M7	M6.5	2780	0.12	0.017	2.74	17.36	2.31	17.38	0.62	0.55	13.55	...	...	...
382	3 44 30.78	32 02 42.9	M6-M7/60±20	M6.5	2780	0.78	0.018	...	...	2.66	18.92	0.87	0.76	13.72	...	...	...
405	3 44 21.02	32 06 15.8	M8/8	M8	2600	0.00	0.011	3.09	18.27	2.57	18.40	0.59	0.38	13.97	...	...	...
407	3 45 04.09	32 05 00.5	M6.5-M7.5/100±20	M7	2720	1	0.0094	...	...	2.86	19.71	0.88	1.41	13.97	...	...	...
413	3 44 45.71	32 11 08.4	M4.75(LRLL)	M4.75	3052	0.70	0.027	2.32	17.33	2.41	17.42	0.55	0.33	14.01	...	...	14.10
414	3 44 44.33	32 10 34.4	M5.25/7(LRLL)	M5.25	2968	0.02	0.010	2.41	17.73	2.34	17.73	0.50	0.61	14.03	0.59	0.39	14.28
415	3 44 29.95	32 09 37.8	M6-M7/250±30(LRLL)	M6.25	2810	0.38	0.016	2.57	18.23	2.80	18.35	0.67	0.12	14.03	0.71	0.65	13.76
432	3 44 45.81	32 03 54.2															

TABLE 1—*Continued*

ID	$\alpha$ (2000)	$\delta$ (2000)	Spectral Type/ $W_\lambda(\text{H}\alpha)$ <sup>a</sup>	Adopt	$T_{\text{eff}}$ <sup>b</sup>	$A_J$	$L_{\text{bol}}$	$R - I$ H98	$I$	$R - I$ this work	$I$	$J - H$	$H - K$ LL	$K$	$J - H$	$H - K$ LRLL	$K$
----	-----------------	-----------------	---	-------	-------------------------------	-------	------------------	----------------	-----	----------------------	-----	---------	---------------	-----	---------	-----------------	-----

<sup>a</sup> Optical spectral types and  $W_\lambda(\text{H}\alpha)$  derived in this work, in addition to optical and IR classifications from LRLL. Some of the LRLL spectral types have been revised slightly. Spectral types of Herbig 1998 (H98) are only shown for three sources where I have no optical data. Measurement uncertainties in spectral types and  $W_\lambda(\text{H}\alpha)$  are  $\pm 0.25$  subclass and  $0.5\text{--}1$  Å, respectively, unless otherwise noted.

<sup>b</sup> Adopted spectral types converted to  $T_{\text{eff}}$  with the dwarf temperature scale in Table 2.

<sup>c</sup> The IR photometry includes a companion while the optical data resolves the two sources.

NOTE.—Sources of photometry include Herbig 1998 (H98), Lada & Lada 1995 (LL), and Luhman et al. 1998b (LRLL).